RSC Sustainability

ROYAL SOCIETY OF CHEMISTRY

TUTORIAL REVIEW

View Article Online
View Journal | View Issue

Check for updates

Cite this: *RSC Sustainability*, 2025, **3**, 3358

A minireview on rubber nanocomposites for sustainable supercapacitors

Susmi Anna Thomas, [a] Jayesh Cherusseri *[b] and Deepthi N. Rajendran [a]

Received 2nd April 2025
Accepted 1st June 2025

DOI: 10.1039/d5su00234f

rsc.li/rscsus

The recent advancements in electronic gadgets necessitate the use of flexible electrochemical energy storage devices to power them. Supercapacitors are the best choices, but the availability of flexible electrode-active materials with excellent electrochemical charge storage capacity is a major bottleneck. The present review discusses the synthesis of flexible electrodes using rubber nanocomposites for supercapacitor applications. This is the first report in the literature on the use of rubber nanocomposites for supercapacitor application. Rubber and their derivatives are used as additives for the fabrication of nanocomposites in both electrode-active materials and electrolytes. Initially, this review discusses the properties of rubber nanocomposites, and then, their various synthesis methods are explained. Furthermore, the preparation of electrode-active materials using rubber nanocomposites, particularly for

[a]*Department of Physics, Government College for Women (Affiliated to University of Kerala), Thiruvananthapuram, Kerala 695014, India*

[b]*Department of Chemistry (BK21 FOUR), Research Institute of Advanced Chemistry, Gyeongsang National University, Jinju 52828, South Korea. E-mail: drjayeshpuli@gmail.com*

Susmi Anna Thomas

Susmi Anna Thomas is a PhD scholar at the Department of Physics, Government College for Women, Thiruvananthapuram, affiliated to the University of Kerala, Thiruvananthapuram, Kerala, India. She completed her Master of Science (MSc) degree with a specialization in Physics in 2018 from Mar Ivanios College, Thiruvananthapuram (affiliated to the University of Kerala), Kerala, India. She also obtained a Master of Philosophy (MPhil) in Physics (University first rank holder) from the Noorul Islam Centre for Higher Education, Tamil Nadu, India, in 2020. Dr Thomas is a recipient of prestigious INUP project awarded by the Ministry of Electronics and Information Technology (MeitY), Government of India, for carrying out the experimental work at the Centre for Nano Science and Engineering (CeNSE), Bangalore, during her PhD. She has published more than 40 research articles and 9 book chapters with an h-index of 17 and an i10-index of 29. Her current research focuses on the development of new-generation two-dimensional layered materials such as transition metal chalcogenides and their applications in electrochemical energy storage devices such as rechargeable batteries and supercapacitors. She is a reviewer of several top listed peer-reviewed journals such as Journal of Energy Storage, Journal of Alloys and Compounds, and ACS Applied Energy Materials.

Jayesh Cherusseri

Jayesh Cherusseri completed his Master's degree (MSc) in Physics, followed by a Master's degree (MTech) in Nanomedical Sciences. He obtained a PhD with a distinction in Materials Science from the Indian Institute of Technology (IIT) Kanpur, India in 2017. He was a recipient of Dr D. S. Kothari post-doctoral fellowship from India in 2017 and the University of Central Florida (UCF) post-doctoral fellowship in 2018. He has published more than 100 research publications including research articles and book chapters. He holds an h-index of 32 and an i10-index of 59, with more than 3500 citations. He has two Indian and one US patent to his credit. He was a recipient of the prestigious Brainpool Fellowship from NRF South Korea in 2024. Dr Cherusseri is currently working as a Brainpool Fellow at Gyeongsang National University, Jinju, South Korea. He was listed in the Stanford University/Elsevier's List of Top 2% Scientists in the World. He is a reviewer of several top-listed journals in the world, such as Nature Communications, Advanced Materials, Advanced Functional Materials, ACS Nano, Progress in Materials Science, Journal of Energy Chemistry, etc. His current research focuses on the synthesis and electrochemical applications of new-generation ultrathin materials.

Open Access Article. Published on 05 2025. Downloaded on 2026/5/17 12:30:56.
This article is licensed under a Creative Commons Attribution-NonCommercial 3.0 Unported Licence.

© 2025 The Author(s). Published by the Royal Society of Chemistry

Open Access Article. Published on 05 2025. Downloaded on 2026/5/17 12:30:56.
This article is licensed under a Creative Commons Attribution-NonCommercial 3.0 Unported Licence.

supercapacitor applications, is elucidated. The evaluation of the electrochemical performance of rubber nanocomposite-based electrodes and supercapacitors is also explained with the help of cyclic voltammetry, electrochemical impedance spectroscopy, and galvanostatic charge/discharge measurement analyses. Rubber nanocomposites are suitable candidates for fabricating supercapacitor electrodes as they possess the high tensile strength, natural abundance, flexibility, environmentally friendly and low cost.

Sustainability spotlight

UN Sustainable Development Goal 7 (affordable and clean energy) manifests the importance of sustainable electrochemical energy storage devices such as supercapacitors for use in next-generation electronic wearables. Polymer nanocomposite-based supercapacitor electrodes exhibit high energy density and flexibility, which are mandatory for the current and next-generation electronic wearables. Rubber nanocomposites are potential candidates for application in flexible and wearable supercapacitors both as a matrix for electrode-active materials and as an electrolyte binder. Highly flexible rubber nanocomposite-based supercapacitors can be used in electronic textiles to supply power to on-body electronic devices.

1. Introduction

The burgeoning urbanization and population explosion resulted in water and energy scarcity worldwide.[1–3] Improved living standards and population growth have led to an increase in the energy demand. Until the end of the 19th century, the energy demand was primarily met by fossil fuel resources.[4–6] Later on, the increase in global warming and related climate change introduced wide range of environmental concerns in the utilization of fossil fuels.[7,8] Accordingly, the use fossil fuels as the primary sources of energy has reduced in the recent past owing to the associated carbon dioxide pollution and global climate change.[9,10] To meet the global energy demands and for a better future, the scientific community has been devoting consistent efforts to develop advanced renewable and sustainable technologies. Consequently, energy production from renewable energy resources has become a point of attraction for energy researchers. The most available renewable energy resources include solar, tidal and wind energies; however, their intermittent nature of energy production is a major bottleneck. The energy generation from these renewable sources is primarily weather dependent; hence, they are not promising sources to deliver continuous power output.[11,12] Therefore, development of highly efficient energy storage devices is an urgent need. Rechargeable batteries and electrochemical capacitors (otherwise known as supercapacitors or ultracapacitors) have emerged as potential electrochemical energy storage devices in the recent past owing to their enhanced charge storage capacity.[13] Although rechargeable batteries such as lithium-ion batteries are the best candidates to achieve high energy density, their major demerit lies in the low power density.[13] However, the long cycle life, wide range of operating temperatures, and high power density introduced *via* rapid charge/discharge processes has attracted the attention of researchers and industry experts towards supercapacitors. The development of high-performance supercapacitors is necessary for high-end power applications such as electric vehicles.

The main components of a supercapacitor are electrode-active materials (positive and negative), current collectors, electrolytes, electrolyte separator membranes, and sealing materials.[14–16] Among these components, the electrode-active materials play major roles in determining the charge storage performance of the supercapacitor.[17] Based on the charge storage mechanisms, the supercapacitors are divided into three major groups: electric double-layer capacitors (EDLCs), pseudocapacitors (or redox capacitors), and battery-type hybrid supercapacitors (otherwise known as supercapatteries).[18] Electric double-layer capacitors store charges by the formation of a double layer of charges at the electrode/electrolyte interface, hence electrode-active materials with a large surface area are a prerequisite to achieve high performance.[19] Examples are carbon nanomaterials such as carbon nanotubes (CNTs) and graphenes. As the name implies, the charge storage in EDLCs is by means of non-faradaic mechanisms, *i.e.*, there will be no charge transfer reactions occurring at the electrode-active materials. Hence, the EDLC electrodes exhibit good electrochemical stability and are best candidates for use in durable applications. In the case of pseudocapacitors, the charges are stored by the redox reactions, materials such as electronically conducting polymers and transition metal oxides are the best

Deepthi N. Rajendran

Deepthi N. Rajendran completed her Master's degree (MSc) in Physics, followed by a Master of Philosophy degree in Physics from the University of Kerala, Thiruvananthapuram, Kerala, India. She obtained her PhD in Physics from the University of Kerala, India, in 2007. She has published more than 60 research publications to date. Her current research focuses on the development of nanomaterials for energy applications, especially in solid oxide fuel cells and supercapacitors. Dr Deepthi is currently working as an Associate Professor and Research Guide at the Department of Physics, Government College for Women, Thiruvananthapuram, Kerala, India. Seven PhDs were produced under her guidance and five students are presently pursuing PhD under her supervision.

Open Access Article. Published on 05 2025. Downloaded on 2026/5/17 12:30:56.
This article is licensed under a Creative Commons Attribution-NonCommercial 3.0 Unported Licence.

materials ever used.[20] Since the charge storage mechanism is by redox reactions, there will be chemical reactions occurring at the electrode surface and that eventually leads to the degradation of the electrodes after a certain number of charge/discharge cycles. This is inevitable since the charge storage is by means of faradaic reactions and the life cycle of the pseudocapacitors are less than that of EDLCs. Supercapatteries are novel electrochemical energy storage systems similar to supercapacitors in which one of the electrodes is a supercapacitor electrode, mostly composed of carbon materials, and the other is a battery-type electrode, mostly composed of materials possessing battery-type charge storage, *i.e.*, charge storage by diffusion-controlled mechanisms. The materials that possess battery-type charge storage are transition metal dichalcogenides, particularly transition metal sulfides such as nickel sulfide, cobalt sulfide, and tin sulfide.[21–24]

The individual electrode-active materials possess demerits, which lead to low specific capacitance and low energy and power densities. Electronic modulation by methods such as doping and nanostructuring is a viable strategy to enhance the charge storage performance of the electrode-active materials.[25–27] However, it is difficult to achieve an enhanced charge storage performance for practical applications. This issue can be overcome by preparing nanocomposites and hybrid/heterostructures with different types of electrode-active materials. By combining two or more different types of electrode-active materials, the individual limitations will be overcome and the synergistic effect of individual components gives rise to enhanced charge storage capacity and long-term stability. The preparation of nanocomposites and hybrid/heterostructure helps in enhancing the charge storage capacity by combining different types of charge storage materials in a single electrode, hence the specific capacitance gets improved multiple times when compared to that of individual materials.[28] The charge storage performance of nanocomposite electrodes is enhanced due to the change in their electrode nanostructure and surface morphology, more electrode-active materials exposed to electrolyte ions to take part in the electrochemical reactions, porous architecture that allows easy penetration of the electrolyte ions, enhanced electronic and ionic conductivities, *etc.*[29] Polymer-based nanocomposites have gained great research interest in the recent past due to their flexibility, reliability, easy processing routes available, and low cost.[30–32] Various types of polymers are used to fabricate the nanocomposite electrodes with electrode-active materials such as carbon nanomaterials, metal oxides, and transition metal dichalcogenides.[33] In a nanocomposite electrode, an optimal content of filler materials is mandatory to achieve the best performance when using them as electrode candidates in supercapacitors.[34,35] In the case of battery-type electrode-active materials, diffusion path lengths have a great influence on the intercalation/deintercalation of electrolyte ions through the electrode nanostructure. Hence, layered materials are highly preferred for the battery-type charge storage since the electrolyte ions can be easily migrated through the electrode nanostructure without any hindrance.[36,37]

Flexible and wearable electronic devices have gained great research interest in the recent past due to their fantastic applications in our daily life including on-body wearables, synthetic skins, and Internet-of-Things (IoTs)-based health-care monitoring systems.[38] These wearable electronic devices require flexible energy storage devices to supply power to them. In this aspect, most of the energy storage devices such as rechargeable batteries and supercapacitors fail in performance as most of these devices are rigid and not able to bend at different bending angles based on the situation. However, rechargeable batteries such as lithium-ion batteries are not safe to use in wearable electronic devices due to the use of lithium and flammable organic electrolytes in them. Hence, flexible supercapacitors using water-based electrolytes gained great research interest. Flexibility is one of the major parameters which depends on the practical application of a supercapacitor for electronic wearables. Thus, it is necessary to introduce materials which provide flexibility, without diminishing their electrochemical performance as well as long-term cycling stability. The major demerit of using supercapacitors is the achievement of output voltage, which is limited to the dissociation potential of water.[39] Hence, supercapacitor modules should be developed by connecting individual supercapacitors in series and parallel combination in order to obtain the voltage and specific capacitance with respect to the practical requirement. The charge storage performance of supercapacitor electrodes can be enhanced by preparing nanocomposite electrodes composed of two or more different types of electrode-active materials. In general, EDLCs exhibit a lower specific capacitance than pseudocapacitors due to the type of charge storage possessed by them.[40]

Natural rubber (NR) is harvested by tapping the bark of the rubber tree (*Hevea brasiliensis*), which releases a milky white liquid called latex. This latex is then processed through coagulation, where acid is added to extract the rubber, and excess water is removed. The resulting rubber is then rolled into sheets or other forms for use in various applications. The NR exhibits high elasticity, good abrasion resistance, resilience, good availability, and low cost.[41–43] This NR can be incorporated with the electrode-active materials in order to prepare nanocomposite electrodes for application in supercapacitors. This not only imparts flexibility to the electrode active material but also provides good mechanical strength as well as stretchability to the supercapacitor manufactured. To avoid the difficulty associated with the rigidity of high-performing supercapacitors, the fabrication of high-performance stretchable electrodes composed of NR is a facile approach.[44] Rubber nanocomposite-based supercapacitors provide high performance as well as flexibility, which can be easily integrated with flexible and wearable electronic textiles to supply power. This imparts flexibility, the supercapacitor can be made as thin as possible and these devices can also be stretchable during applications such as bending and stretching.

The flexibility and stretchability without any performance alteration are the unique features of rubber nanocomposites for various applications. There is a great demand for the rubber nanocomposites for a wide variety of applications, which is evident from the statistical representation of a number of

© 2025 The Author(s). Published by the Royal Society of Chemistry

Open Access Article. Published on 05 2025. Downloaded on 2026/5/17 12:30:56.
This article is licensed under a Creative Commons Attribution-NonCommercial 3.0 Unported Licence.

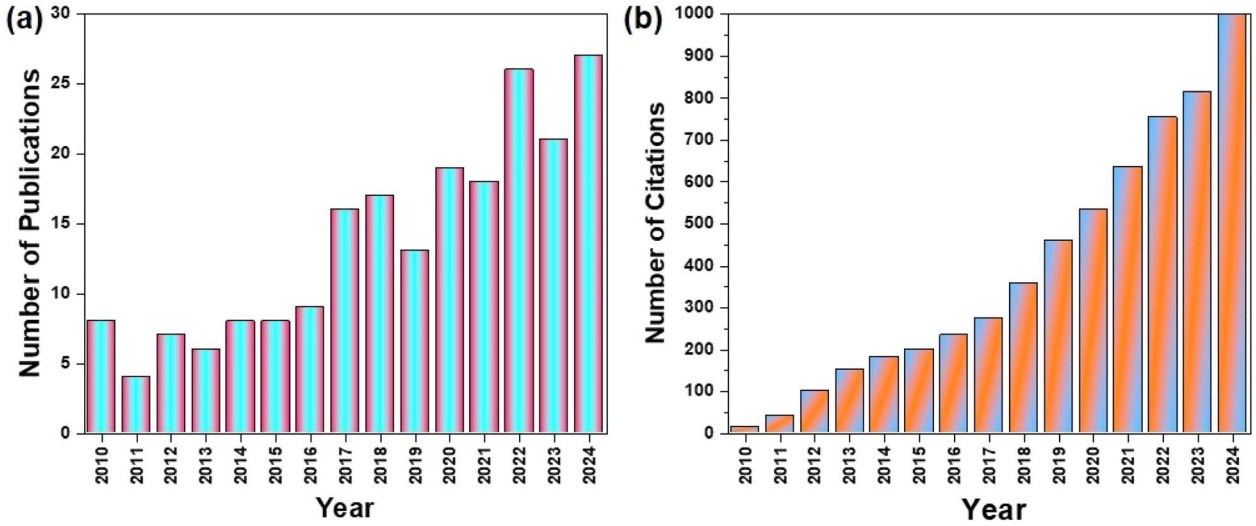

Scheme 1 (a) Number of publications and (b) number of citations received in the area of rubber nanocomposites for energy storage applications in the literature from 2010 to 2024 (Source: Web of Science, Keyword: "Rubber nanocomposites for energy storage").

publications based on rubber nanocomposites for energy storage applications reported in the literature from 2010 to 2024, as depicted in Scheme 1a. The number of citations received for these publications for the past 15 years is depicted in Scheme 1b. The statistics shows that the potential applications of rubber nanocomposites are increasing day by day, particularly in the case of electrode-active materials for supercapacitors. Rubber nanocomposites are widely used as electrode-active materials in flexible and stretchable supercapacitors. However, a review article in this field is lacking in the literature. This has motivated us to write a review on the exemplary application of rubber nanocomposite-based electrodes for supercapacitor applications. The present review deals with the importance of rubber-based electrode materials for supercapacitor applications. We discuss about the application of rubber-based nanocomposites as supercapacitor electrode active materials in polymer matrixes that provide high flexibility in applications. Fig. 1 provides the outline of this review.

Fig. 1 Outline of the review. (a) TEM image corresponds to CNTs (10 wt%) in NR. Reproduced with permission from ref. 45 Copyright (2006) Elsevier Inc. (b) Schematic of the rGO/silica/NR composite prepared *via* a wet compounding procedure. Reproduced with permission from ref. 46 Copyright (2020) MDPI. (c) Digital image of the sample of S48 hydrogel. Reproduced with permission from ref. 47 Copyright (2023) Elsevier Inc. (d) Digital image of the supercapacitor during the stretching experiment. Reproduced with permission from ref. 61 Copyright (2018) MDPI.

2. Properties of rubber nanocomposites

To introduce the multifunctional applications of rubber nanocomposites, a clear understanding of their properties is necessary. This section deals with the fundamental properties of rubber nanocomposites that are important for energy storage applications such as electronic properties, mechanical properties, and optical properties.

2.1 Electronic properties of rubber nanocomposites

The NR exhibits significant electronic properties to meet the demands for electronic devices. However, a cross-linked/vulcanized rubber without using a reinforcement inside the matrix is not appropriate for promising application due to the low electronic conductivity associated with rubber nanocomposites. Electronically conductive rubber composites have gained prominent interest in different fields such as supercapacitors, transistor, and sensors. Elastomeric materials have low electrical conductivity of less than 10^{-11} S m^{-1}. However, the introduction of conductive fillers can increase the electrical conductivity to 10^{-2} S m^{-1}. The prominent electronically conductive character is achieved through the introduction of

Open Access Article. Published on 05 2025. Downloaded on 2026/5/17 12:30:56.
This article is licensed under a Creative Commons Attribution-NonCommercial 3.0 Unported Licence.

a percolation pathway of conductive fillers in matrix, which facilitates increasing the electrical conductivity even at lower concentrations. Hence, there is a high demand for light-weight low-cost alternative nanocomposites when compared to that of traditionally developed rubber nanocomposites with electronically non-conducting fillers. The nanofillers play a crucial role in the modification of the electronic conductivity of rubber composites. There are various types of electronically conductive fillers used such as CNTs, graphenes, and reduced graphene oxide (rGO).

Electronically conducting polymers are another class of electronically conducting materials. The examples of electronically conducting polymers include polypyrrole, polyaniline (PANI), and poly(3,4-ethylenedioxythiophene):polystyrene sulfonate. PANI is a widely explored electronically conducting polymer that is suitable for preparing nanocomposite electrodes for electrochemical energy storage devices such as rechargeable batteries and supercapacitors. One of the major works that can be found from the literature deals with the facile synthesis of PANI@cellulose nanowhisker (CN)/NR nanocomposites having a three-dimensional hierarchical architecture using bio-template synthesis.[48] Here, the layer of PANI is *in situ* synthesized over a cellulose nanofiber template to prepare a PANI@CN nanohybrid having a higher aspect ratio and good dispersivity. After this, the PANI@CN nanohybrid is selectively located at the interfaces of the NR microsphere and organized to a three-dimensional hierarchical network structure with co-coagulation. The morphological studies of the prepared materials are carried out by transmission electron microscope (TEM) imaging, as shown in Fig. 2. The cellulose nanofibers having a needle-like structure with a length ranging from 200 to 500 nm can be observed. After performing the *in situ* polymerization of aniline monomers into a cellulose nanofiber, the PANI@CN nanohybrid shows good dispersion with a rod-like architecture. PANI does not produce a higher degree of aggregation. To evaluate the template effect of cellulose nanofibers, they are self-assembled and coated over NR surface with latex microspheres, and their diameter is in the range of few hundreds of nanometers (Fig. 2a). From this image, it can be inferred that several NR microspheres were encapsulated into the cellulose nanofiber, which is beneficial for the formation of a continuous network with a lower concentration of cellulose nanofibers. The cellulose nanofiber shell was coated into NR microsphere latex which is connecting to each other.

Owing to this, the cellulose nanofiber makes selective localization to interstitials between NR microspheres and organizes to a continuous network, as shown in Fig. 2b. This leads to the formation of an interconnected network, which originated from individual cellulose nanofibers, which act as a prototype for a three-dimensional hierarchical conductive network in the NR matrix. The electrical conductivity delivered by these hybrids is evaluated with undeformed sample by two-point measurement with a resistance meter for $R \leq 2 \times 10^8\ \Omega$ or using a ZC36 high resistance instrument for $R > 2 \times 10^8\ \Omega$. Rectangular strip (40 mm × 10 mm × 1 mm) or square (100 mm × 100 mm × 1 mm) samples were used for electrical studies. Five samples were selected for each individual sample to attain a mean value. The volume resistance, R_v, is converted into volume resistivity, ρ_v, according to ASTM D4496 and D257:

$$\rho_v = R_v \frac{A}{t}$$

where 'A' is the effective area of the electrode in m^2 and 't' is the specimen thickness (in m). The conductivity measurement of PANI/NR and PANI@CNs/NR with different loading amounts of PANI is shown in Fig. 2c. Here, the PANI@CN nanohybrid is synthesized with a constant feeding mass ratio of aniline/CNs, and the resulting mass ratio of aniline/CNs is 1.5/1. An optimal amount of conductive filler required to produce the insulator-to-conductor ratio is known as the 'percolation threshold'. The PANI@CNs/NR nanocomposite shows much reduced electrical conductivity threshold for percolation (3.8 phr at 3.6 vol%) than the PANI/NR composite (8.8 phr at 8 vol%). Moreover, prominent conductivity enhancement is obtained for every sample. The electrical conductivity of the PANI/NR composite with 5 phr PANI is 0.5×10^{-14} S m^{-1}, but in the case of PANI@CNs/NR composite with a similar loading fraction, it reaches 3.8×10^{-3} S m^{-1}, showing a prominent improvement, ~11 orders in magnitude. This improved conductivity is due to the biotemplate comprising CNs and the three-dimensional hierarchical conductive multiscale structure with the NR matrix. The mass ratio of PANI to cellulose nanofiber in the electrical conductivity of the PANI@CNs/NR nanocomposite is investigated through tuning the feeding mass ratio introduced by aniline to cellulose nanofiber during polymerization. The feeding mass ratio of aniline/cellulose nanofiber was 2/1, 4/1, and 8/1. The PANI/cellulose nanofiber final mass ratio was 0.8/1, 1.5/1, and 2.6/1, representing that the quantity of PANI deposited on cellulose nanofibers is increased with the increase in the mass ratio of aniline/cellulose. The influence of the feeding mass ratio of aniline to cellulose nanofiber on the electrical conductivity of PANI@CNs/NR having PANI with 7.5 phr is shown in Fig. 2d. A maximum electrical conductivity of 5.4×10^{-2} S m^{-1} was obtained for the aniline/cellulose nanofiber at a feeding mass ratio of 4/1. When this feeding ratio reduced to 2/1 and increases to 8/1, the conductivity makes a reduction to 2.4×10^{-4} and 2.0×10^{-4} S m^{-1}, respectively. It is observed that the electrical conductivity of this NR-based composite is influenced with the amount of PANI deposited on cellulose nanofibers. The present study demonstrates the influence of additives in the improvement of NR nanocomposites for multifunctional applications. These electronically conducting additives have prominent importance in the performance of elastomers.

2.2 Mechanical properties of rubber nanocomposites

Mechanical features such as tensile strength, stiffness, and resilience are important parameters, which affect the real-time applications of elastomeric materials. The use of pristine NR latex (NRL) possesses low mechanical properties, hence nanofillers are extremely important to strengthen their mechanical properties. The properties of filler materials such as large surface area, good electronic conductivity, and mass are important parameters that determine the properties of the resulting

© 2025 The Author(s). Published by the Royal Society of Chemistry

Open Access Article. Published on 05 2025. Downloaded on 2026/5/17 12:30:56.
This article is licensed under a Creative Commons Attribution-NonCommercial 3.0 Unported Licence.

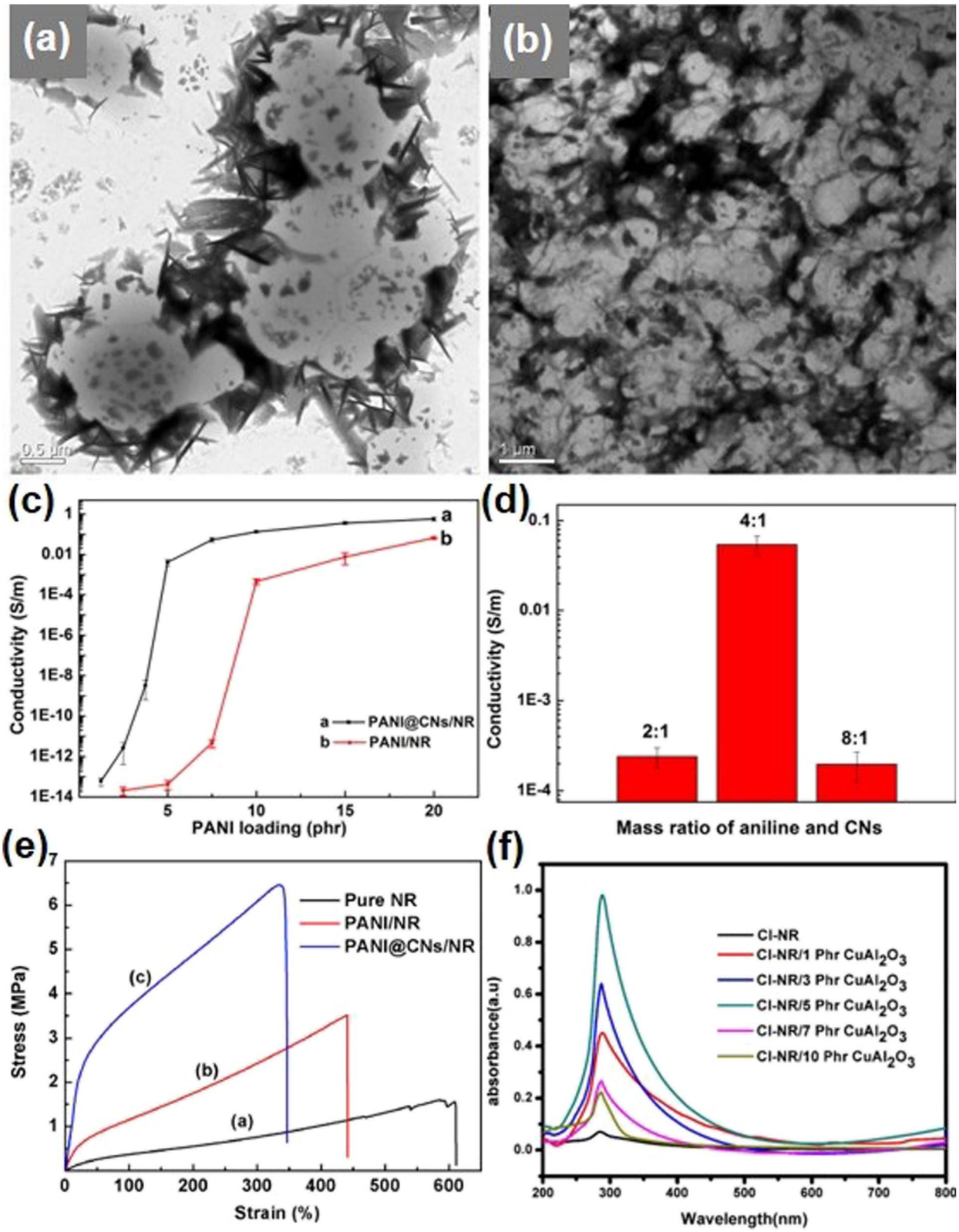

Fig. 2 (a and b) TEM images of cellulose nanofiber/NR nanocomposites synthesized with cellulose nanofibers and NRL microspheres; (c) electrical conductivity variation in the PANI@CNs/NR nanocomposite with respect to PANI loading; (d) influence of the feeding mass ratio of aniline and cellulose nanofibers on the electrical conductivity of the PANI@CNs/NR nanocomposite with 7.5 phr PANI; (e) stress–strain curve of the pure NR, PANI/NR nanocomposite, and PANI@CNs/NR nanocomposite. Reproduced with permission from ref. 48 Copyright (2014), the American Chemical Society. (f) Ultraviolet-visible spectra of Cl-NR and composites with varying contents of $CuAl_2O_3$ nanoparticles. Reproduced with permission from ref. 49 Copyright (2022), Springer Nature.

Open Access Article. Published on 05 2025. Downloaded on 2026/5/17 12:30:56.
This article is licensed under a Creative Commons Attribution-NonCommercial 3.0 Unported Licence.

nanocomposite material. The advancements in the field of electronic wearables necessitate flexible and wearable electrodes for their development. Among the various options available, rubber nanocomposites with improved mechanical properties are inevitable for flexible electrode fabrication. A work which relates to the fabrication of wearable sensors with pre-vulcanized NR and epoxidized NRL added with graphene oxide (GO), graphene powder, graphene pastes and rGO is an example.[50] The authors of this work prepared various rubber nanocomposites with varying graphene components and analysed its performance. The tensile strength of these rubber nanocomposites was evaluated using an Instron machine with 10 N load cell capacity operating at room temperature. From this experiment it is observed that an efficient loading for GO-incorporated pre-vulcanized rubber latex is at 1.5 phr having sonication similar to the pre-vulcanized NR/graphene powder. The occurrence of graphene in pre-vulcanized rubber was found to improve the mechanical features of the rubber nanocomposites. Thus, it was found that graphene in pre-vulcanized rubber improved the mechanical properties of rubber latex and can be used for a variety of applications. In the case of epoxidized NR 50 latex, the percolation point is taken at a less amount of reduced filler loading of <0.1 phr. However, the values of other combinations are not good in comparison with the performance shown by epoxidized NR 50 latex with graphene components. The increase in the mechanical features held by epoxidized NR 50 latex is due to the mobility held by graphene grown over the surface of NR perfectly. Thus, this study introduced the feature of graphene in the enhancement of mechanical properties of NR nanocomposites. The tensile strength of PANI@CNs/NR nanocomposites having a three-dimensional hierarchical architecture is found to be superior to that of pure NR and PANI/NR,[48] as shown in Fig. 2e. These results indicate the effect of fillers on the tensile properties of NR. For the NR, the tensile strength is 1.7 MPa, but for PANI@CNs/NR nanocomposites, it is increased to be about 267.3% (6.1 MPa) and for the PANI/NR nanocomposite, it is 3.4 MPa (an increase of ~103.0%). Young's modulus of PANI@CNs/NR is about 10.7 MPa and it is found to be 29.7 times greater than that of the pristine NR (0.4 MPa) and 4.6 times greater than that of the PANI/NR nanocomposite (2.3 MPa). Hence, it can be said that the PANI@CN hybrid is an efficient candidate in the NR reinforcement due to the higher tensile strength and Young's modulus of CNs. The increase in dispersity obtained for the PANI@CN nanocomposite is due to the bio-template effect produced by the CNs, which enhances the mechanical strength of the NR. Elongation at the breaking point of PANI/NR and PANI@CN/NR nanocomposites is lower than that of the pristine NR, which is common for all the nanocomposite materials prepared with filler components. These results show that the bio-template preparation and latex co-coagulation route help in improving the electrical conductivity and mechanical strength of NR composites.

2.3 Optical properties of rubber nanocomposites

The optical features of rubber nanocomposites have significant attention in various fields such as in luminescent devices and light-emitting diodes. The optical properties of rubber nanocomposites were investigated by scientists by studying the effects of chemical modifications such as epoxidation, hydrogenation, chlorination and dehydrohalogenations on non-polar rubber for improving the compatibility with the polar filler and nonpolar diene rubber for the modification of electrical, optical and mechanical features. Among the various chemically modified rubber nanocomposite samples, the chlorinated elastomer exhibits high flame resistance, chemical resistivity, adhesive architecture and mechanical feature compared to the parent polymer with respect to the occurrence of electronegative chlorine segments in the diene rubber backbone. Chlorinated NR (Cl-NR) nanocomposites with different contents of zinc ferrite nanoparticles were synthesized by a roll mill approach.[51] From ultraviolet-visible absorption spectroscopy, the Cl-NR exhibits a characteristic π–π^* transition peak observed at 320 nm. There occurs a peak shift from 320 nm toward 324, 325, 288, 323, and 284 nm when loaded with 1, 3, 5, 7, and 10 phr zinc ferrite nanoparticles, respectively. The shifting of peak toward a higher wavelength is due to the efficient nanofiller incorporation inside the polymer matrix. Among the various combinations, a nanofiller with 5 phr was found to exhibit a uniform distribution within the Cl-NR matrix. The nanocomposite with a broad peak indicates the nanoparticles in random arrangement, but a sharp peak indicate the uniform arrangement of nanofillers within the rubber matrix. The nanocomposite having 10 phr concentration holds low-wavelength absorption due to the agglomerated fillers within it. This composite shows an increase in absorbance intensity with a filler loading of 5 phr, representing the intermolecular interaction of the filler and chlorinated matrix. There is a report based on the unvulcanised NR/copper alumina nanocomposite by a two-roll mixing approach.[49] The ultraviolet-visible spectra recorded for the Cl-NR and its composite are shown in Fig. 2f. Here, the Cl-NR occupies a π–π^* transition peak at 286 nm possesses a low intensity. From this figure, it is clear that the Cl-NR/$CuAl_2O_3$ nanocomposites exhibit a peak in the high-wavelength region due to the efficient incorporation of $CuAl_2O_3$ in the Cl-NR matrix. The peak shift from 286 nm toward a higher wavelength clearly indicates the type of interaction between the $CuAl_2O_3$ nanofiller and the Cl-NR matrix. At 5 phr $CuAl_2O_3$ loading, the absorption peak exhibits a higher intensity, introducing an adequate filler concentration within the Cl-NR matrix. However, at a higher loading more than 5 phr, the peak with reduced intensity can be observed, as the interfacial adhesion of polymer components decreases at a higher loading in accordance with the high filler–filler interaction than the filler–polymer interaction. There exists a structural alteration for the Cl-NR with respect to an increase in $CuAl_2O_3$ loading.

3. Synthesis methods of rubber nanocomposites

There are different methods available for the preparation of rubber nanocomposites such as solution mixing, mechanical/melt mixing, and latex mixing. This section discusses these various methods with their importance in designing specific

© 2025 The Author(s). Published by the Royal Society of Chemistry

Open Access Article. Published on 05 2025. Downloaded on 2026/5/17 12:30:56.
This article is licensed under a Creative Commons Attribution-NonCommercial 3.0 Unported Licence.

rubber nanocomposites with different types of nanofillers that can be manufactured on a larger scale.

3.1 Synthesis of rubber nanocomposites by solution mixing

The solution mixing process involves the mixing of polymer solution and nanofiller dispersion together by ultrasonication, shear mixing or stirring. After this procedure, the polymer/nanofiller dispersion obtained is taken for casting in a mold and kept for evaporation of the solvents. NR nanocomposites were prepared by a solution mixing approach by Fakhru'l-Razi *et al.* in which multi-walled CNTs (MWCNTs) were used as the nanofillers using toluene as the solvent.[45] The MWCNT introduced with concentration such as 1, 3, 5, 7, and 10 wt% by maintaining the overall mass of the nanocomposite as 10 g. The procedure involved in the preparation of NR/MWCNT nanocomposite can be divided into four steps. The first step is the preparation of MWCNT dispersion, and it involves MWCNT dissolution/dispersion in a toluene solvent in order to disentangle the individual nanotubes. These nanotubes are typically clinging together and introduce lumps, which make processing difficult. In order to resolve this, a certain amount of MWCNTs are introduced into a specific quantity of toluene solution after careful weighing. The prepared solution was then kept for sonication, to introduce effective nanotube dispersion. In this present study, the authors prepared solutions by varying the

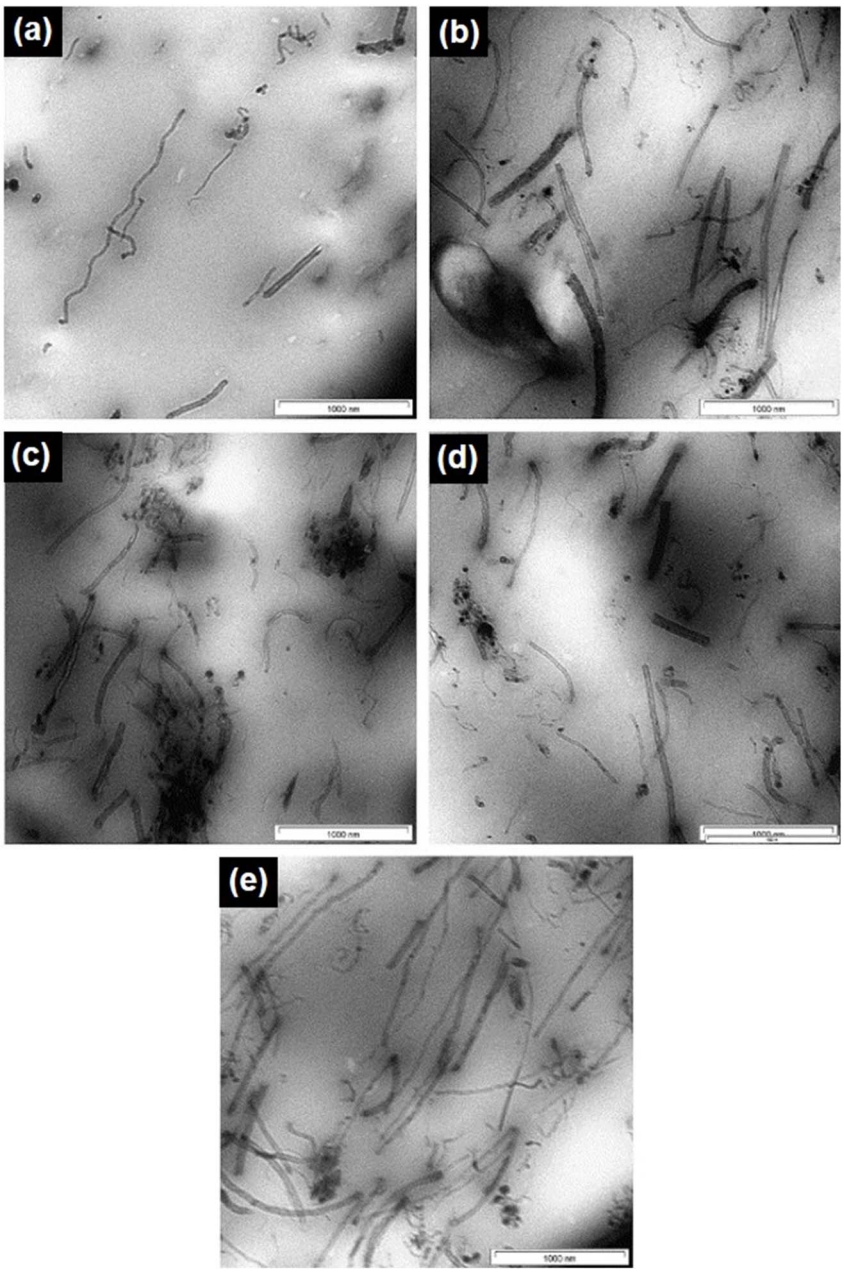

Fig. 3 TEM images corresponding to CNT in the NR nanocomposite. CNTs with (a) 1 wt%, (b) 3 wt%, (c) 5 wt%, (d) 7 wt%, and (e) 10 wt%. Reproduced with permission from ref. 45 Copyright (2006), Elsevier Inc.

Open Access Article. Published on 05 2025. Downloaded on 2026/5/17 12:30:56.
This article is licensed under a Creative Commons Attribution-NonCommercial 3.0 Unported Licence.

concentration of MWCNTs such as 1, 3, 5, 7, and 10 in 10 mL toluene. In the second step, the dissolution of NR in toluene was carried out. In a typical procedure, 10 g NR is introduced into 500 mL of toluene and undergoes stirring until it makes a uniform dispersion. In the third step, the melt preparation was carried out, by mixing of two solutions prepared in previous steps to blend the MWCNTs in NR. Finally, the nanocomposite comprising the NR and MWCNTs were pressed using a hot press and cut to a standard shape. The microstructure and dispersion of MWCNTs in the NR are verified by TEM imaging, and the corresponding TEM images are depicted in Fig. 3. From Fig. 3a, it can be observed that both the short and long MWCNTs are dispersed within the NR matrix. A homogeneous distribution of MWCNTs in the NR can be observed. The MWCNTs are open at both ends during the dispersion of MWCNTs in toluene, with the aid of ultrasonic frequency vibration and mechanical stirring. The range of distance between the individual MWCNTs in the matrix is observed to be wide and oriented with good interface interaction between them. The diameter of individual MWCNTs is in the range of 2–20 nm with both short and long nanotubes. Fig. 3b shows the TEM image of the nanocomposite having 3 wt% MWCNTs in the NR matrix, and the orientations of MWCNTs are found to be randomized. Fig. 3c–e show MWCNTs in the NR matrix having concentrations of 5, 7, and 10 wt%, respectively. The TEM images clearly indicate that an increase in the concentration of MWCNTs in NR makes the orientations of nanotubes more randomized. The MWCNT orientations influence the mechanical properties of the nanocomposite. The solution mixing process is an efficient route for the preparation of rubber nanocomposites, but the removal of solvents is found to be a serious concern in it.

3.2 Synthesis of rubber nanocomposites by mechanical/melt mixing

In this method, nanocomposite fabrication is performed using an internal mixer such as ball-mill and two roll-mill. An experimental work carried out by Sharif *et al.*[52] signifies the importance of mechanical/melt mixing approach in the preparation of rubber nanocomposites by considering NR/clay composites. NR/clay composites are prepared through melt mixing using a Haake internal mixer at a temperature of 120 °C. Here the speed of the rotor is set at 60 rpm for 10 minutes. The composites are compression molded at a temperature and pressure of 120 °C and 110 kg cm^{-2}, respectively. The prepared sample sheets are having a dimension of 150 mm × 150 mm × 1 mm. The irradiation is performed in air using a Cockroft Walton-type electron beam accelerator at 2 MeV acceleration voltage having a beam current of 5 mA, and the rate of dose is set to be 50 kGy per pass. The organoclay sodium montmorillonite is modified with cationic surfactants such as dodecyl ammonium chloride and octadecylamine ammonium chloride. The XRD analysis revealed that the silicate layer dispersion in the NR matrix show regular arrangement of silicate layers in both the pristine/intercalated form and an irregular arrangement during the complete layer exfoliation. The sodium

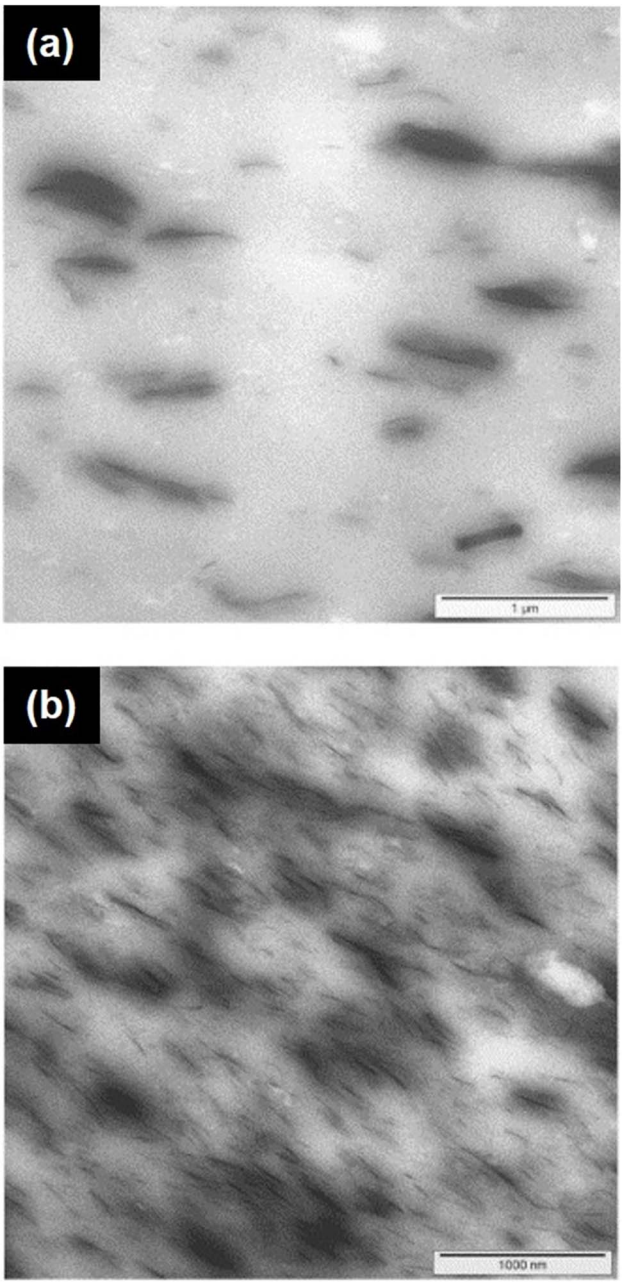

Fig. 4 TEM images of an (a) NR with DDA clay and (b) NR with ODA-modified clay. Reproduced with permission from ref. 52 Copyright (2005), Elsevier Inc.

introduced clay have an interlayer distance of 1.22 nm, and it is expanded to 1.38, 1.32, 1.31, and 1.25 nm for the case of NR containing 1, 3, 5, and 10 phr sodium-modified clay. The hydrophilic character of sodium-modified NR is highly affected by NR intercalation. The TEM images displayed in Fig. 4a and b show that the NR with dodecyl ammonium chloride-modified clay has exfoliated lamellae and tactoids consisting of different numbers of lamellae and tactoid aggregates. However, the NR with octadecylamine ammonium chloride-modified clay exhibited a uniform distribution of silicate layers in it without any possible clay aggregation.

© 2025 The Author(s). Published by the Royal Society of Chemistry

Open Access Article. Published on 05 2025. Downloaded on 2026/5/17 12:30:56.
This article is licensed under a Creative Commons Attribution-NonCommercial 3.0 Unported Licence.

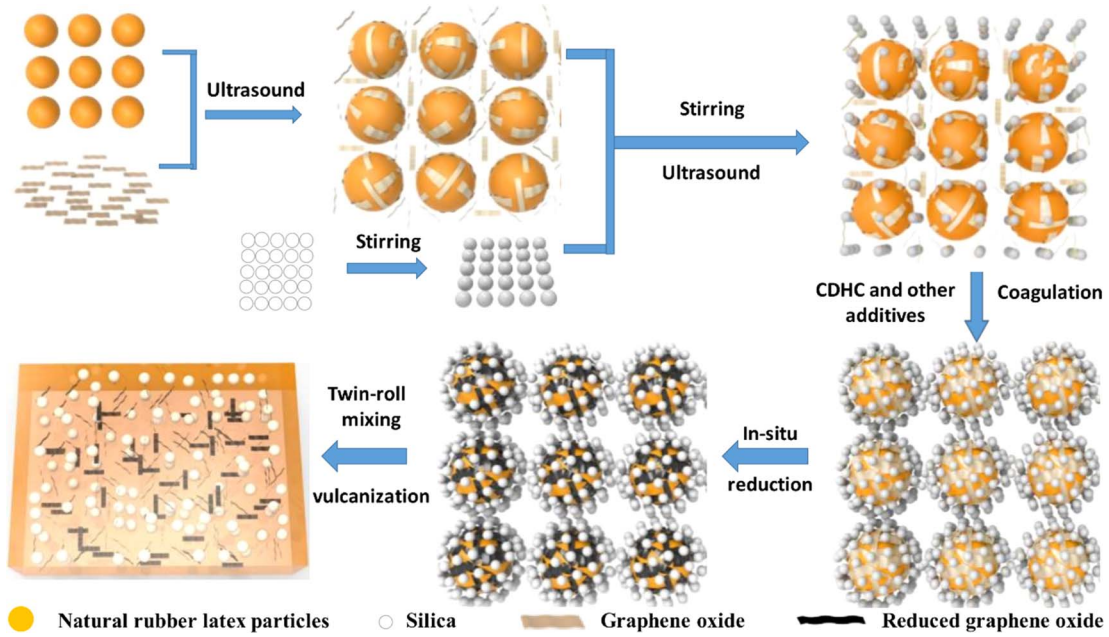

Fig. 5 Wet compounding procedure combined with an ultrasonic-assisted latex mixing route for preparing rGO/SiO_2/NR nanocomposites. Reproduced with permission from ref. 46 Copyright (2020) MDPI.

The mechanical/melt mixing approach is appropriate for industrial processes since this procedure has the merits of environment-friendliness, low cost, fast production, high efficiency and large-scale production. This method is solvent-free and stands as a major substitute for the solution mixing procedure. However, one of the major drawbacks of mechanical/melt mixing is the application of higher temperature, as it adversely influences the stability of nanofillers and surface functionalization. The processing of any material at a higher temperature is always a major demerit. The compatibility of nanofillers and polymers during the processing influences the properties of the prepared nanocomposites. There is a chance for reduction in the uniform dispersion of fillers in the matrix when the viscosity of the matrix is very high or when there is a higher filler loading.

3.3 Synthesis of rubber nanocomposites by latex mixing

In this approach, elastomers are used in the latex form and this method is environmentally friendly and cost-effective. Through a latex mixing approach, it is possible to prepare a uniform dispersion of rubber nanocomposites without any possible aggregation or agglomeration. In order to prove the feasibility of the latex mixing approach for the synthesis of rubber nanocomposites, NR modified-rGO filled with a higher content of silica (SiO_2) is demonstrated.[46] Initially, nanosized SiO_2 nanoparticles are dispersed in deionized water by ultrasonication and mechanical stirring at room temperature. Then, a definite quantity of GO is dispersed in deionized water using an ultrasonic bath at a temperature of 25 °C for 3 h to prepare an aqueous dispersion of GO. Later, NRL was taken and mixed with a GO solution under sonication for a period of 2 h. Further, the SiO_2 dispersion is introduced inside the rubber latex mixture during which it was agitated with ultrasonic and mechanical mixing for a period of 2 h. Furthermore, the other vulcanization additives containing surfactants are kept for pre-emulsification using a high-speed mixer, and it is introduced and dispersed in a latex mixture through ultrasonication and stirred for a duration of 2 h. Cystamine dihydrochloride solution is added dropwise into the latex mixture for coagulation and hydrazine hydrate was introduced into the system with ultrasonic and mechanical stirring for a duration of 2 h at a temperature of 60 °C, to reduce GO into rGO. The resulting coagulated SiO_2/rGO/NR solid sample is filtered, washed several times with water and placed in an oven for vacuum drying at a temperature of 60 °C for a duration of 30 h. The SiO_2/rGO/NR solid is mixed for a duration of 5 minutes in an open twin roll-mill at room temperature having a fraction ratio of 1/1/1 and a nip gap of around 0.5 mm. Later, the SiO_2/rGO/NR solid underwent compressive molding for a temperature and pressure of 150 °C and 15 MPa, respectively, for optimum curing time, and it is cooled under a pressure of 10 MPa at room temperature for a duration of 30 minutes to prepare various vulcanized samples. The schematic representation of the synthesis procedure is given in Fig. 5. From the morphological analysis using TEM, the authors of this work observed that there exists a uniform dispersion of both SiO_2 and rGO. Even at a higher concentration of SiO_2, rGO makes good dispersion within the NR matrix. It is found that rGO make a preferable orientation within the NR matrix other than the embedded SiO_2 nanoparticles.

4. Applications of rubber nanocomposites in supercapacitors

Based on the electrode configuration, supercapacitors are divided into three categories: symmetric, asymmetric, and battery-type hybrid supercapacitors.[53] Nanocomposite

Open Access Article. Published on 05 2025. Downloaded on 2026/5/17 12:30:56.
This article is licensed under a Creative Commons Attribution-NonCommercial 3.0 Unported Licence.

electrodes are the most widely used ones in fabricating a supercapacitor due to their improved conductivity, high specific capacitance, good chemical and electrochemical stability, *etc.* A symmetric supercapacitor makes use of both its electrodes of the same type, whereas in the case of an asymmetric supercapacitor, both the electrodes are of different types based on the nature of charges possessed by them. In general, activated carbon is an example of the negative electrode used in an asymmetric supercapacitor. In a battery-type hybrid supercapacitor, the positive electrode possesses diffusion-controlled charge storage, hence named 'battery-type'. Due to the flexibility, rubber nanocomposites become potential electrode candidates for application in supercapacitors. The NRL contains *cis*-1,4-polyisoprene and non-rubber-type components, which easily make a polymer linkage to other materials during the preparation of supercapacitor electrodes.[54,55] GO is a prominent candidate for supercapacitor electrode fabrication, which contains an sp^2 hybridized planar carbon sheet with a large surface area and a higher number of oxygen-containing surface functional groups.[56] The introduction of GO to NRL latex helps in improving the thermal, mechanical and electrical properties of the electrode-active material. However, there are less studies reported based on the influence of various properties such as the thermal, mechanical and electrical properties of the electrode-active material for supercapacitor applications. The GO/NRL nanocomposite synthesized by an electrochemical exfoliation route was used as an electrode-active material for supercapacitors.[57] In this work, GO was synthesized by a one-step approach using sodium dodecyl sulfate with 0.01 M concentration. GO and NRL were mixed in a volume ratio of 1/1 *via* stirring and bath sonication for a duration of 2 h followed by drop-casting onto a 5 cm × 5 cm container. Then, the resulting drop-casted sample was dried overnight. A two-step process was also adopted to compare the microstructure and surface

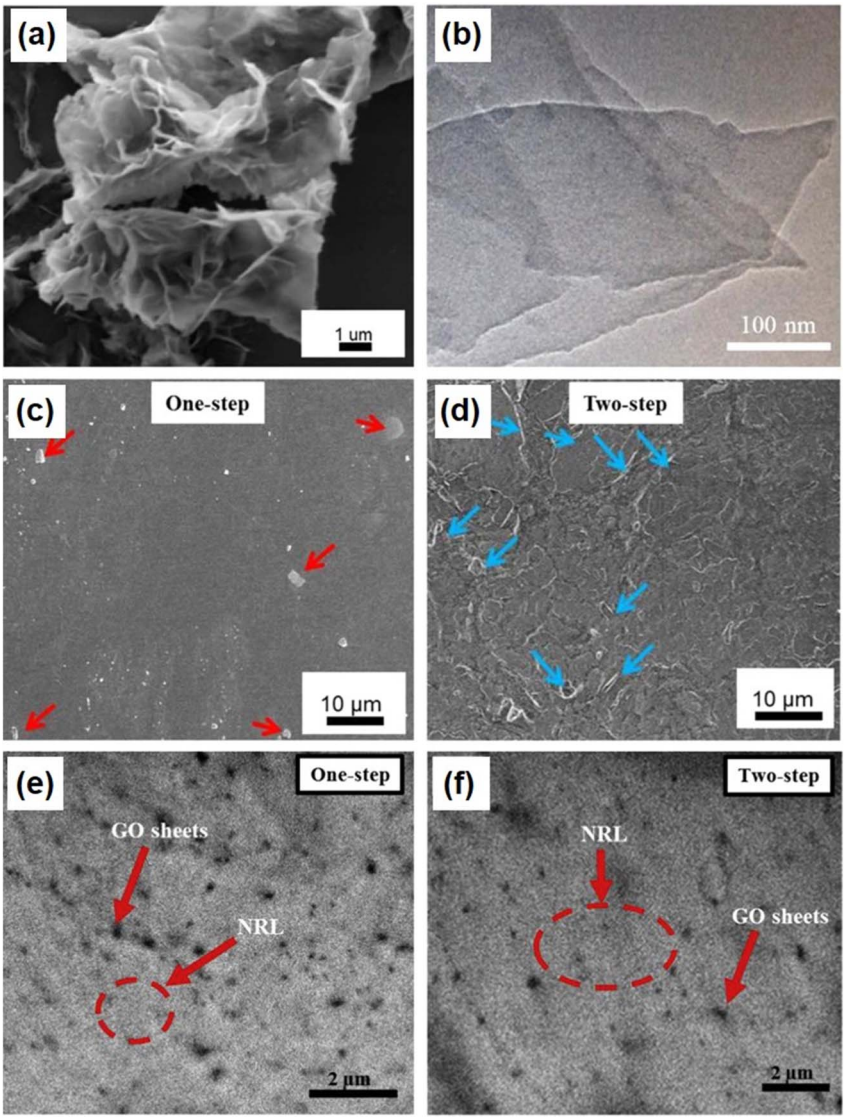

Fig. 6 (a) FESEM and (b) HRTEM images of pristine GO; (c and d) FESEM and (e and f) HRTEM image of the GO/NRL nanocomposite. Reproduced with permission from ref. 57 Copyright (2015), Elsevier Inc.

© 2025 The Author(s). Published by the Royal Society of Chemistry

Open Access Article. Published on 05 2025. Downloaded on 2026/5/17 12:30:56.
This article is licensed under a Creative Commons Attribution-NonCommercial 3.0 Unported Licence.

morphology of the GO/NRL nanocomposite with the traditional method. The field-emission scanning electron microscope (FESEM) image of GO (Fig. 6a) shows a rose petal-like architecture having a thin and almost transparent sheet. The oxidation is the reason behind the wavy architecture in GO. High-resolution TEM (HRTEM) image confirms the ultrathin nature of GO (Fig. 6b). The oxidation on GO confirmed the presence of oxygen-containing surface functional groups *via* the Fourier-transform infrared (FTIR) spectrum and an absorption peak observed at 230 nm in the ultraviolet-visible spectrum.

After performing a one-step intermixing of GO into NRL, a fair smooth surface having agglomerated GO is obtained (Fig. 6c). The interfacial interaction between GO and NRL is denoted by red arrows. The authors of this work confirmed it using FTIR spectroscopy analysis too in which a reduced intensity for the hydroxyl group originated from the interaction between NRL and oxygen-containing surface functional groups on the GO sheets. However, a rough and fractured surface in the nanocomposite can be observed, which was synthesized by a traditional mixing approach (Fig. 6d). The aggregation of GO nanosheets as a result of inhomogeneous distribution of GO nanosheets in the NRL matrix is represented by blue arrows. The HRTEM image of the nanocomposite synthesized *via* a one-step approach (Fig. 6e) shows the uniform dispersion of GO nanosheets when compared to that of the one prepared by conventional mixing (Fig. 6f). The charge storage characteristics of the as-prepared GO/NRL nanocomposite electrodes were evaluated by cyclic voltammetry (CV) analysis. The CV profiles obtained for the GO/NRL nanocomposite electrodes prepared by one-step and two-step mixing methods within a fixed potential window of 0.0–1.0 V are depicted in Fig. 7a and b, respectively. The CV curves display pseudocapacitive charge storage possessed by the GO/NRL nanocomposite electrodes. The specific capacitance for the GO/NRL nanocomposite electrodes synthesized by a one-step method was calculated to be 103.7 F g^{-1}, whereas it was only 32.6 F g^{-1} for the one synthesized *via* a two-step method. The authors of this also conducted the current–voltage analysis and calculated the conductivity of both the GO/NRL nanocomposite electrodes. A high conductivity of 7.12×10^{-5} S cm^{-1} was obtained for the GO/NRL nanocomposite electrode synthesized by a one-step method, whereas it was only 3.62×10^{-7} S cm^{-1} for the one prepared by a two-step method. The agglomeration of graphene nanosheets as well as the homogeneous distribution of graphene nanosheets within the NRL matrix is responsible for the conducting channels, which in turn gives rise to an enhanced conductivity and the redox-active GO is responsible for the high specific capacitance. These results indicate that the designing of the electrode material for supercapacitors and the synthesis steps adopted influence the charge storage characteristics of supercapacitors.

With respect to this higher electrochemical performance delivered by the GO/NRL composite, the authors illustrated a mechanism behind its formation. The OH and O radicals introduced from H_2O anodic oxidation open the edge sheet *via* an oxidative cleavage reaction. This facilitates the non-covalent intercalation of surfactants having a hydrophilic tail group within the graphite layer. The weaker bonding force present between graphite layers introduced exfoliation and GO sheet precipitation. After preparing the GO solution, the NRL is subsequently mixed, the same as in a two-step approach. The surfactant's hydrophilic headgroup is forced to interact with NRL particles that are covered through positive and negative charges in protein and phospholipid molecules. The NRL is making a direct linkage and self-arrangement along the surfactant tail surface coated by GO. However, in the case of a conventional mixing approach, there is one tail group connecting GO and NRL, at an interaction ratio of 1/1. In comparison with the one-step approach, there exists an increase in electrical conductivity through tail numbers connecting GO and NRL. This is introduced due to the negative charge in the hydrophilic headgroup that initially directed to NRL, providing sufficient interaction between GO and NRL before the surfactant tail is intercalated into the graphite layer. By this approach, the interaction between GO and NRL increases, in comparison to the two-step route. This interaction exists between GO and

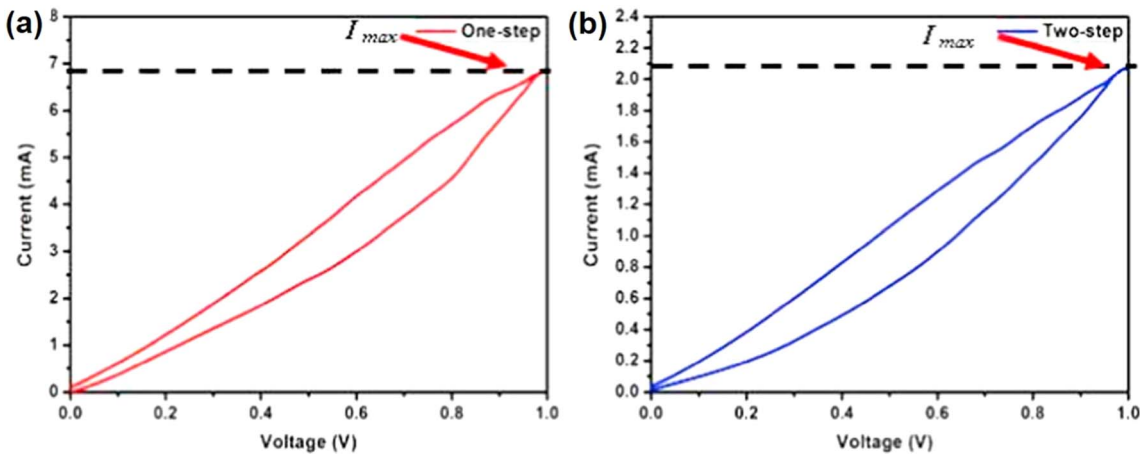

Fig. 7 CV profiles of the GO/NRL nanocomposite electrodes prepared *via* the (a) one-step mixing method and (b) two-step mixing method. Reproduced with permission from ref. 57 Copyright (2015), Elsevier Inc.

Open Access Article. Published on 05 2025. Downloaded on 2026/5/17 12:30:56.
This article is licensed under a Creative Commons Attribution-NonCommercial 3.0 Unported Licence.

NRL is further increased during intermixing by supplying power at 5 V. Thus, the GO/NRL nanocomposite prepared *via* the facile one-step approach exhibits efficient electrical and capacitive performance with respect to the two-step route. The present study demonstrates the potential application of GO/NRL nanocomposites in supercapacitors.

A comparative analysis was conducted on the one-step and two-step synthesis procedure of GO/NRL nanocomposites, and the electrical features of the nanocomposites were evaluated to use them as efficient electrode materials for supercapacitor fabrication.[58] Here, the GO/NRL nanocomposite was prepared with SDS as the surfactant and NRL as the natural polymer. Different concentrations of SDS were used ranging from 0.001 to 1.000 M to obtain a highly optimized GO/NRL nanocomposite with efficient electrical characteristics. At the same time, the NRL polymer volume incorporated in nanocomposite production is fixed at a volume ratio of 1/1 of GO dispersion. With respect to GO dispersion introduction in the NRL polymer, there is a prominent increase in measured conductivity (2.33×10^{-9}–5.08×10^{-7}) S cm^{-1} in comparison to the NRL polymer (in the order of 10^{-12} S cm^{-1}). Here, 0.01 M of SDS-GO/NRL polymer nanocomposite is synthesized through one-step approach, which shows a higher conductivity of 7.12×10^{-5} S cm^{-1} with respect to the nanocomposite prepared with 0.1 M (2.59×10^{-7} S cm^{-1}), 1.0 M (4.92×10^{-8} S cm^{-1}) and 0.001 M SDS (4.42×10^{-9} S cm^{-1}). A high conductivity was obtained when 0.01 M SDS is used and it can be due to the optimized GO dispersion and higher interconnectivity between the individual GO sheets. An increase in conductivity observed for the GO/NRL nanocomposite is obtained by GO structure variation having a large number of wrinkles influencing the proper dispersion of GO in the nanocomposite, which allows an efficient conductive pathway within the NRL matrix. Additionally, the concentration of surfactant plays a role in the generation of a percolating pathway between GO sheets, and it is more essential to render insulating NRL for the production of nanocomposites with electrically conducting GO. The GO/NRL nanocomposite is fabricated *via* a conventional two-step approach. From the *I–V* curve of a 0.1 M SDS-GO/NRL polymer nanocomposite prepared *via* a two-step approach, it is found that this combination possesses a higher conductivity of 5.08×10^{-7} S cm^{-1}. Later, it is analysed with a sample prepared with 0.01 M SDS concentration and it shows a conductivity value of 3.62×10^{-7} S cm^{-1}. The 0.001 M SDS-GO/NRL nanocomposite sample exhibits a low conductivity of $\sim 2.33 \times 10^{-9}$ S cm^{-1}. In comparison to the GO/NRL nanocomposite prepared by a one-step approach, the nanocomposite synthesized by a two-step procedure exhibits low conductivity. This occurred due to a reduced diffusion rate of GO to NRL matrix, which results from reduced interaction between the GO and NRL in the nanocomposite synthesized *via* a two-step process. The utilization of a high electrolyte concentration of SDS greater than 0.1–1.0 M for GO production resulted in lower interaction between the GO and NRL for the nanocomposite prepared by a two-step approach. Using an SDS electrolyte having a high electrolyte concentration greater than 0.1–1.0 M to produce GO results in a reduced electrical conductivity of 2.37×10^{-8}–4.92×10^{-8} S cm^{-1}, which occurs through GO agglomeration produced at a given electrolyte concentration. The high electrical conductivity value of GO/NRL nanocomposite prepared for SDS concentration of 0.01 and 0.1 M made it as a suitable candidate for supercapacitor analysis and they evaluated the electrochemical performance of it. In the CV curve, there exists a slight deviation from the rectangular shape to a leaf-like structure, which indicates the pseudocapacitive charge storage. The specific capacitance obtained for the supercapacitor electrode prepared with a 0.01 M SDS GO/NRL nanocomposite *via* a one-step approach is 107 F g^{-1}, which is observed to be higher than that of the nanocomposite prepared by a two-step method (32.6 F g^{-1}). In the case of 0.1 M SDS-GO/NRL composite synthesized by one- and two-step approaches, the specific capacitance is observed to be 80 and 0.4 F g^{-1}, respectively. This prominent difference in capacitance observed between the nanocomposite electrodes prepared by a two-step approach by using 0.01 and 0.1 M SDS produces a reduced current response in the range of 1.08 μA–2.10 mA in comparison to the nanocomposite synthesized by a one-step approach (6.9–8.0 mA). These results confirm that the procedure to fabricate a GO/NRL nanocomposite influences the charge storage performance of the supercapacitor electrode. The high degree of agglomeration in GO (0.1 M SDS) is due to the availability of oxygen-containing surface functional groups attached to the GO sheets, which restricts the ionic diffusion pathways, thereby causing less interaction between the electrode and the electrolyte.

There are some demerits in the application of NRL for practical application due to its viscous nature, heat sensitivity, reduced solvent resistance, *etc.*[59] Thus, the vulcanization of NRL is a favourable route and it is performed *via* two approaches such as sulfur vulcanization and radiation vulcanization. The radiation vulcanization method is the preferred and most commonly used method for the cross-linking of rubber than the sulfur vulcanization approach. The radiation vulcanization involves the higher penetration of gamma rays from a radioactive source, that is ^{60}Co, and the acceleration of lower energy electron beam from the electron accelerator. This radiation-vulcanized NRL (RVNRL) has reduced cytotoxicity and higher degradable character as well as low emission of sulfur dioxide than that in the case of a sulfur-vulcanized NRL. The synthetic RVNRL, used in zinc-free or non-sulfur vulcanization systems, has a higher thermal stability and modulus strength to resistance. RVNRL was established in the early 1950's itself, which satisfies a higher level of end-product application than that of sulfur-vulcanized NRL.

By understanding the features of RVNRL, researchers adopted a two-step method to prepare a rGO/RVNRL nanocomposite for the preparation of supercapacitor electrodes.[60] In a typical procedure, hydrazine hydrate is used as a reducing agent for GO to obtain rGO. The hydrazine hydrate is added to a GO solution and mixed in a volumetric ratio of 1/100 and the preparation of rGO/NRL nanocomposite is carried out by stirring and ultrasonication. In addition to this, the rGO/RVNRL nanocomposite is also prepared with SDS as the surfactant. Here, 0.1 M SDS is used to prepare GO, and it takes 24 h. The resulting SDS and GO dispersion undergo stirring and sonication by the RVNRL

© 2025 The Author(s). Published by the Royal Society of Chemistry

Open Access Article. Published on 05 2025. Downloaded on 2026/5/17 12:30:56.
This article is licensed under a Creative Commons Attribution-NonCommercial 3.0 Unported Licence.

matrix introduction before cast drying overnight. The nanocomposite is prepared by using another surfactant, 1,4-bis(-neopentyloxy)-3-(neopentyloxycarbonyl)-1,4-dioxobutane-2-sulfonate (TC14), and it is observed that ~4.15–4.3 wt% of GO and rGO is consumed during the preparation of TC14-GO/RVNRL and TC14-rGO/RVNRL nanocomposites. After performing reduction, the conductivity of the TC14-rGO/RVNRL nanocomposite is obtained to be 1.32×10^{-3} S cm^{-1}, which is greater than that of the TC14-GO/RVNRL nanocomposite (2.65×10^{-4} S cm^{-1}). These results show that the conductivity of nanocomposites prepared using the surfactant TCl4 is much higher than that prepared with SDS, which is ~1.79×10^{-5} S cm^{-1}. The results obtained show that the reduced surface tension of TC14 tripletail surface above the particular critical micelle concentration level in RVNRL matrix leads to an efficient adsorption on rGO sheet thereby creates highly conductive nanocomposites in comparison with the SDS. From CV measurements, it is observed that the TC14-rGO/RVNRL nanocomposite electrode exhibits a specific capacitance of 95 F g^{-1} at a scan rate of 100 mV s^{-1} whereas it is 63 F g^{-1} for the TC14-GO/RVNRL nanocomposite electrode. These results unveil the high efficiency of rGO for the charge storage over GO due to high electronic conductivity. The introduction of the RVNRL polymer contributes to a slight increase in the charge transfer resistance of the rGO/RVNRL nanocomposite electrode. In addition, a wrinkled architecture in the prepared rGO sheets exhibit efficient accessibility to the electrolyte ions, which not only make penetration to the outer portion of rGO but towards its inner region also, in comparison to higher agglomeration occurring in GO sheets. Moreover, the rGO/RVNRL nanocomposite electrode exhibits good wettability obtained *via* the residual functional groups present on rGO sheets, therefore it increases the amount of hydrophobic polar sites. By incorporating GO and rGO in the RVNRL matrix, a less cracked surface was observed in the case of the TC14-GO/RVNRL nanocomposite. The TC14-rGO/RVNRL nanocomposite shows efficient distribution of rGO sheets with few aggregations, which is caused by reduced affinity introduced between rGO sheets due to the usage of TC14. For comparison, the nanocomposite of rGO/RVNRL assisted through SDS surfactants has higher agglomerated rGO sheets, as a result of reduced effective interaction between SDS–rGO dispersion and RVNRL matrix. Using HRTEM imaging, the authors of this work observed that the GO/RVNRL assisted with TC14 surfactants shows more agglomerated GO sheets with respect to rGO/RVNRL, where a well dispersed rGO was observed in the as-prepared nanocomposite. However, in the nanocomposite prepared using SDS, there exists a higher agglomeration of rGO sheets that gives rise to a reduced conductivity to the nanocomposite.[60]

Stretchable supercapacitors become a fascinating energy storage device, particularly for electronic wearables. The indispensable component in a stretchable supercapacitor is the highly flexible and stretchable electrode that have the capability to deliver high power as well as impart flexibility. Apart from the advantageous features of stretchable supercapacitors, there exist some demerits, which hinder the fabrication of a stretchable supercapacitor with high mechanical durability. Initially, the electrode-active material-coated substrate should possess a higher degree of tolerance to strain. To resolve these problems, different structures are introduced, which include the electrode-active material fabricated on a polymetric film substrate, coating the electrode-active material on a textile fabric, and wrapping of electrode-active materials on elastic polymer fibers. Second, the mechanical robustness and stability of other components of supercapacitors such as current collectors and electrolytes during stretching need to be guaranteed. The point is the necessity to develop a simpler fabrication method to prepare and assemble the stretchable supercapacitor. Without meeting these requirements, a stretchable supercapacitor is not able to operate accurately under harsh mechanical conditions such as stretching deformation. Recently, there are various methods established for the fabrication of stretchable supercapacitors. Single-walled CNTs (SWCNTs) or graphene deposited over a buckled rubber substrate can be used as stretchable electrodes for supercapacitor fabrication. The electro-active material-coated substrate used for the fabrication of stretchable supercapacitors is necessary to promote higher electrical conductivity and adequate elasticity.

A stretchable supercapacitor based on electrospun elastic rubber nanofibrous mats with SWCNTs is reported in the literature.[61] In this work, poly(styrene-*b*-butadiene-*b*-styrene) (SBS) is used as an electrospun nanofiber due to its good elasticity and a highly stretchable silicone gel (Ecoflex) mixture is used as the substrate. Ecoflex exhibits a Young's modulus of ~60 kPa, which is observed to be softer than commonly used polydimethylsiloxane (PDMS), which affords highly improved mechanical features during stretching. By simple dipping and drying procedures, SWCNTs are deposited over electrospun SBS. Since the coating process has a higher influence on the surface features of the SBS nanofiber, utmost care needs to be given for the surface treatment during the processing. The electrochemical performance evaluation of supercapacitors is carried out in 1-ethyl-3-methylimidazolium bis(trifluoromethylsulfonyl)imide electrolyte. In a typical procedure, the electrode preparation process involves SWCNT coating over SBS nanofibrous mats, which are attached to an Ecoflex film through gentle pressing to achieve good adhesion. Due to the tacky behaviour of the Ecoflex surface, the SWCNT coated on the SBS nanofiber mat is firmly attached to the rubber surface and it acts as a porous electrode. In addition, the SBS nanofibrous mat is immersed in [EMIM][NTf2], which act as a separator between a pair of identical Ecoflex/SBS nanofibrous with SWCNT-coated mat electrodes. To assure proper electrical contact, a copper strip is attached to the edge portion of each of the SWCNT-coated SBS fiber mat electrode and a clip was placed in the middle of each cell. The assembled supercapacitor is mounted onto the custom-made stage for stretching and electrochemical analysis. The aqueous SWCNT solution dispersed in various surfactants hardly wet the nanofiber surface of SBS due to the efficient intrinsic hydrophobic character of SBS. In addition to this, the rugged surface present in the SBS nanofiber enhances its hydrophobicity. Consequently, to coat SWCNTs, wetting characteristics need to be improved with proper surface

Open Access Article. Published on 05 2025. Downloaded on 2026/5/17 12:30:56.
This article is licensed under a Creative Commons Attribution-NonCommercial 3.0 Unported Licence.

treatment that increases the surface energy of the SBS nanofibrous mat. The morphological features of the SWCNT/SBS nanofibrous mat were examined after three various treatments of the SBS nanofiber surface: ultraviolet ozone (UVO), polydopamine coating, and fluorinated surfactant (Zonyl) treatments. These proposed methods are widely established to increase the surface wettability, which leads to improved adhesion. After the UVO treatment, SWCNTs do not make uniform adherence to the surface of the SBS nanofiber. This is due to the rugged surface in the SBS nanofibrous mat, which does not make UVO to reach its surface within a three-dimensional fibrous matrix. For polydopamine coating, nanofiber films are simply immersed in a dopamine solution under basic conditions, which results in decorating polydopamine on the fiber surface. A uniform SWCNT coating is achieved by this method when compared to the UVO treatment. Finally, the SBS nanofiber surface was treated by a fluorinated surfactant, Zonyl. The SBS nanofiber film with Zonyl treatment is carried out by dipping the SWCNT in a Zonyl solution. The changes present in the wetting characteristics of the SWCNT for a Zonyl-treated SBS nanofiber are prominently different from the untreated SBS nanofiber mat. In addition, the SWCNT density on the SBS nanofiber was found to be higher than that of the other two methods followed, such as UVO treatment and polydopamine treatment. The SWCNT layer number is generally about 1–2 layers on the SBS nanofiber, resulting in a SWCNT thickness of ~10–40 nm. The electrochemical analysis of the supercapacitor electrode is evaluated in a two-electrode cell configuration. The CV analysis is performed at different scan rates ranging from 0.005 to 0.1 V s^{-1}. The CV curves thus obtained exhibit a rectangular shape with symmetric nature at all scan rates, which indicates high reversibility during the charge/discharge process. Volumetric capacitances of 12.8, 9.8, 5.6, and 4.3 F cm^{-3} were obtained at scan rates of 0.005, 0.01, 0.05, and 0.1 V s^{-1}, respectively. Galvanostatic charge/discharge (GCD) measurements were performed for the supercapacitor and a slight deviation from the typical linear relationship between the time and potential at different current densities was observed. The authors of this work evaluated the supercapacitor performance under various strain rates. By stretching the supercapacitor to 0%, 20%, and 40% of strain, the CV curves (Fig. 8a) have maintained their original shape, indicating that there is no prominent change or damage occurring even in the liquid atmosphere in the inner portion of the device. However, when the supercapacitor stretched at a higher strain of 50%, a change in CV curve in terms of a reduced area under the curve was observed. Since the area under the CV curve is a measure of the charge storage possessed by the supercapacitor, at a higher applied strain, the charge storage of the supercapacitor got diminished. The GCD curves obtained at different applied strains such as 0%, 20%, and 40% exhibit a deviation from the typical linear charge/discharge character (Fig. 8b). The experimental set-up used to test the stretch in the supercapacitor is given in Fig. 8c. Hence, it can be said that the tolerable stretching is below 40% of applied strain. The volumetric capacitance calculated at a current density of 0.021 A cm^{-3} is

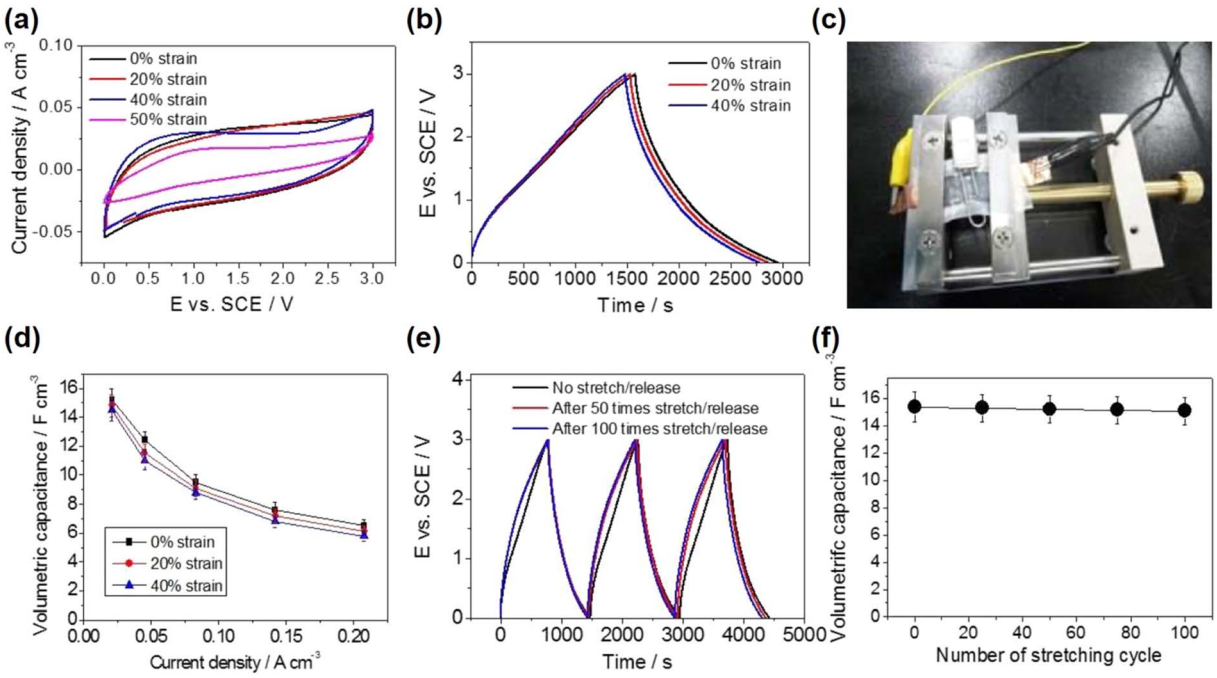

Fig. 8 Electrochemical performance of the supercapacitor during stretching; (a) CV curves at different applied strains of 0%, 20%, and 40%; (b) GCD curves at different applied strains of 0%, 20%, and 40%; (c) photograph of the supercapacitor stretching experimental setup; (d) volumetric capacitance at different current densities at different applied strains of 0%, 20%, and 40%; (e) GCD curves at a current density of 0.045 A cm^{-3} for 0, 50, and 100 times repeated stretch/release cycles at an applied strain of 40%; and (f) change in volumetric capacitance during the stretching exercise (0, 25, 75, and 100) of stretch/release cycles. Reproduced with permission from ref. 61 Copyright (2018) MDPI.

© 2025 The Author(s). Published by the Royal Society of Chemistry

Open Access Article. Published on 05 2025. Downloaded on 2026/5/17 12:30:56.
This article is licensed under a Creative Commons Attribution-NonCommercial 3.0 Unported Licence.

found to be 15.2, 14.8, and 14.5 F cm^{-3} at an applied strain of 0%, 20%, and 40%, respectively. This indicates that the fabricated device has good capacitance retention even at an applied strain of 40%. A reduction in volumetric capacitance is observed upon increasing the current density at an applied strain of 40% when compared to that of the 0% strain (unstretched condition), as shown in Fig. 8d. This may be due to the ineffective ion dissociation/accumulation in the SWCNT/SBS porous nanofiber mat electrode. Moreover, the functionality of device remains under better conditions. The GCD curves obtained at different cycle numbers such as 1st, 50th, and 100th during the repeated stretch/release cycles performed at a constant current density of 0.045 A cm^{-3} with an applied strain of 40% are shown in Fig. 8e. The variation in the volumetric capacitance obtained at different cycle numbers during the stretch/release exercise is depicted in Fig. 8f, from which it can be inferred that there was only 1% capacitance loss at its 50th and 100th cycles when compared to that of the first one. This stretching exercise clearly shows the harsh mechanical deformation and the high robustness of the supercapacitor fabricated with the SWCNT/SBS porous nanofiber mat electrodes. The supercapacitor possesses a volumetric energy density of 2–5.6 mWh cm^{-3} and a volumetric power density of 158–1450 mW cm^{-3} at a current density in the range of 0.021–0.208 A cm^{-3}, respectively.

Synthetic or polar NRL exhibits high mechanical strength. Low-temperature exfoliated GO incorporated with different types of NRL-based nanocomposites such as GO/NRL, GO/RVNRL and GO/epoxy NRL 25 (ENRL25) and their electrochemical performances were studied recently.[62] The use of GO without any stabilization process results in a reduced dispersion level within the NRL nanocomposite. To avoid this, the authors of this work used a hyperbranched triple-tail surfactant, TC14. The proposed TC14 surfactant helps in the exfoliation, intercalation, and stabilization of GO nanosheets in an aqueous solution during the electrochemical exfoliation procedure. The GO/NRL and GO/RVNRL nanocomposites are synthesized by a one-step electrochemical exfoliation procedure. In a typical procedure, a TC14-GO : NRL ratio of 1 : 1 is used at an applied voltage of 7.0 V for 2 h before performing cast drying overnight. Mechanical stirring and bath sonication are adopted for the preparation of both GO/NRL and GO/ENRL25 nanocomposites. Before preparing the nanocomposite of GO with NRL, the surface morphological features of GO are studied, which possess a wavy architecture of separate graphitic sheets due to efficient oxidation by an electrochemical exfoliation approach. The FESEM analysis of GO/NRL, GO/RVNRL, and GO/ENRL25 nanocomposites is analysed. There occurs an introduction of bump-like GO particles, which make an uneven distribution in the nanocomposite. This is due to the high van der Waals interaction for GO itself and a low GO–NRL interaction. Bigger GO particles agglomerated are pulled out from the NRL interface, thus a slight reduction in electrical conductivity is obtained for the GO/NRL nanocomposite. There occur fractures and fewer crack surfaces in the GO/RVNRL nanocomposite. In the case of the GO/ENRL25 nanocomposite, a crumpled morphology is observed for the GO sheet. The incomplete insertion of a polar group in epoxy into the interlayer spacing of GO sheet results in the GO layer pull out from the nanocomposite. However, the GO/ENRL25 nanocomposite exhibits efficient interaction in comparison to that of the GO/NRL nanocomposite. The GO/NRL nanocomposite having a lower concentration of exfoliated GO leads to the formation of bigger clusters on the nanocomposite surface. This is due to the restacking character of GO itself and reduced covalent interaction between the GO and the NRL matrix. The efficient synergistic effect of GO dispersion stabilized with triple-tails in TC14 surfactant and RVNRL matrix which contributes to improvement in dispersion level in the nanocomposite led to a fracture surface. The fractured surface in the GO/RVNRL nanocomposite proves that an efficient interaction occurs between oxygen functional groups present in the GO sheet and hydroxyl groups and free radicals in the RVNRL matrix. In the case of the GO/ENRL25 nanocomposite, there exists a reduction in the cluster size of GO in comparison to the GO/NRL nanocomposite. This is due to the increase in compatibility and the covalent reaction between the GO dispersion and the ENRL25 matrix because of the presence of an epoxide end group in the ENRL25 matrix. However, there are larger agglomerates of GO sheets in the ENRL25 matrix, resulting in a non-uniform surface in comparison to the GO/RVNRL nanocomposite. The CV analysis of the prepared nanocomposites is performed to investigate the charge storage characteristics within a potential window of 0.0–1.0 V in a 1 M KOH aqueous electrolyte. The GO addition in various nanocomposites prepared in this study is found to enhance the charge storage characteristics. The CV curves show typical redox-type charge storage possessed by the GO in the nanocomposite electrodes. The GO/NRL nanocomposite electrode exhibited a specific capacitance of 30 F g^{-1}, which is higher than that of GO/ENRL25 (10 F g^{-1}) and GO/RVNRL (5 F g^{-1}) nanocomposite electrodes. The variation in the specific capacitance of these nanocomposite electrodes is mainly due to the difference in their conductivities. The wrinkled structure of GO in the NRL matrix in the case of the GO/NRL nanocomposite triggers the faster movement of electrolyte ions, and the presence of various oxygen-containing surface functional groups gives rise to an enhancement in the specific capacitance. These observations agree with high current response achieved through a GO/NRL polymer nanocomposite (~3.5 mA) compared to the GO/ENRL25 (~0.72 mA). The lower charge storage performance of the GO/RVNRL nanocomposite is due to the possession of a higher number of defects present in the RVNRL matrix, which reduce the accessibility to ion penetration in the electrodes.

Methyl-grafted NR (MG49-NR)-based electrolytes are reported for supercapacitor application in the recent past.[63] In this study, the MG49-NR-based electrolyte was prepared with corresponding speciality rubber and natural graphite-based electrode-active materials used for the supercapacitor fabrication. Initially, MG49-NR is cut into small pieces and dissolved in tetrahydrofuran inside a fume cupboard for 12 h. Later, $Zn(CF_3SO_3)_2$ is dissolved in tetrahydrofuran for 24 h. The MG49-NR : $Zn(CF_3SO_3)_2$ composition is fixed to be 1 : 0.6 and a conductivity of 0.6 × 10^{-4} S cm^{-1} is achieved at room temperature. Further, these two solutions are mixed, kept under

Open Access Article. Published on 05 2025. Downloaded on 2026/5/17 12:30:56.
This article is licensed under a Creative Commons Attribution-NonCommercial 3.0 Unported Licence.

magnetic stirring, poured to a Petri dish and left for the evaporation of the solvent in order to make a thin film. The structures of MG49-NR and $Zn(CF_3SO_3)_2$ are schematically shown in Fig. 9a and b, respectively. Attenuated total reflectance FTIR spectroscopy analysis is performed to examine the chemical bonding information of MG49-NR, $Zn(CF_3SO_3)_2$ and MG49-NR + $Zn(CF_3SO_3)_2$ and the transmittance spectra recorded are depicted in Fig. 9c. The prominent region of interest is the oxygen atom present in the carbonyl group (–C═O) positioned at 1740–1700 cm^{-1} and the ether group (C–O–C) located at 1250–1050 cm^{-1}. The symmetric stretching introduced by carbonyl group ν(–C═O) at 1727 cm^{-1} occurs for poly(methyl methacrylate) (PMMA), which causes a slight broadening, and it shifts to 1725 cm^{-1} after blending with a $Zn(CF_3SO_3)_2$ salt. This process confirms the weak stretching mode in the C═O carbonyl group due to efficient intermolecular interaction. However, the bond length of ν(–C═O) in PMMA is long, due to the higher electronegativity of oxygen atoms, which pull Zn^{2+} ions toward central atoms, thus the bond between carbon and oxygen is stretched in the carbonyl group. In addition to this, the proposed intermolecular interaction affects the vibrational band corresponding to the –O–CH_3 group. After incorporating $Zn(CF_3SO_3)_2$ salt into the MG49-NR matrix, there is a shift from 1447 to 1449 cm^{-1}. This blueshift is a signature of strong symmetry stretching between oxygen and methyl groups, confirming the successful formation of the polymer–salt complex. Additionally, the peak positioned at 1147 cm^{-1} corresponds to the asymmetrical ν_{as}(–C–O–C) stretching and the peak located at 1271 cm^{-1} corresponds to the ν_s(–COO–) stretching in MG49-NR, which were found to be shifted toward 1154 and 1278 cm^{-1}, respectively, by the incorporation of a $Zn(CF_3SO_3)_2$ salt. This higher stretching occurs in the electronegativity of double bonds held by carbon with oxygen, and they coordinated by Zn^{2+}. These results indicate a highly efficient intermolecular interaction between the oxygen from the carbonyl group of PMMA in the MG49-NR matrix with Zn ions. The crystallinity of MG49-NR, $Zn(CF_3SO_3)_2$ salt, and MG49-NR + $Zn(CF_3SO_3)_2$ is analysed by XRD analysis, and the spectra obtained are shown in Fig. 9d. The XRD spectra of MG49-NR consist of peaks at 2θ = 29.5°, 36.0°, and 39.5°, which correspond to the PMMA in MG49-NR and it reveals its semicrystalline nature. Moreover, the XRD spectra held by a $Zn(CF_3SO_3)_2$ salt contain peaks at 8.3°, 17.0°, 20.6°, 21.2°, 23.3°, 23.9°, 24.5°, 28.6°, 29.6°, 30.4°, 33.6°, 34.2°, 35.2°, 35.9°, 36.9°, 37.7°, and 39.9°, which confirms the higher crystalline character of salt. By blending with the MG49-NR polymer, the intense peaks at 29.5°, 36.0°, and 39.5 disappear. It is due to the reduction in the semicrystalline architecture held by a polymer salt matrix. There exists a disappearance of peaks hold by $Zn(CF_3SO_3)_2$ blended with MG49-NR. This confirms the good solvation of $Zn(CF_3SO_3)_2$ in the MG49-NR matrix.

A supercapacitor is assembled by sandwiching two similar natural graphite electrodes with the MG49-NR + $Zn(CF_3SO_3)_2$ electrolyte, and the performance is evaluated by CV analysis and GCD measurements. The CV curves of the supercapacitor obtained at different scan rates are shown in Fig. 10a. The CV curves display a typical box-type nature, indicating the EDLC charge storage possessed by the supercapacitor due to the natural graphite electrode. At higher scan rates, the nature of CV becomes different, and a change from the box-type curves toward the highly resistive character can be observed. The poor accumulation of charges at the electrode/electrolyte interface

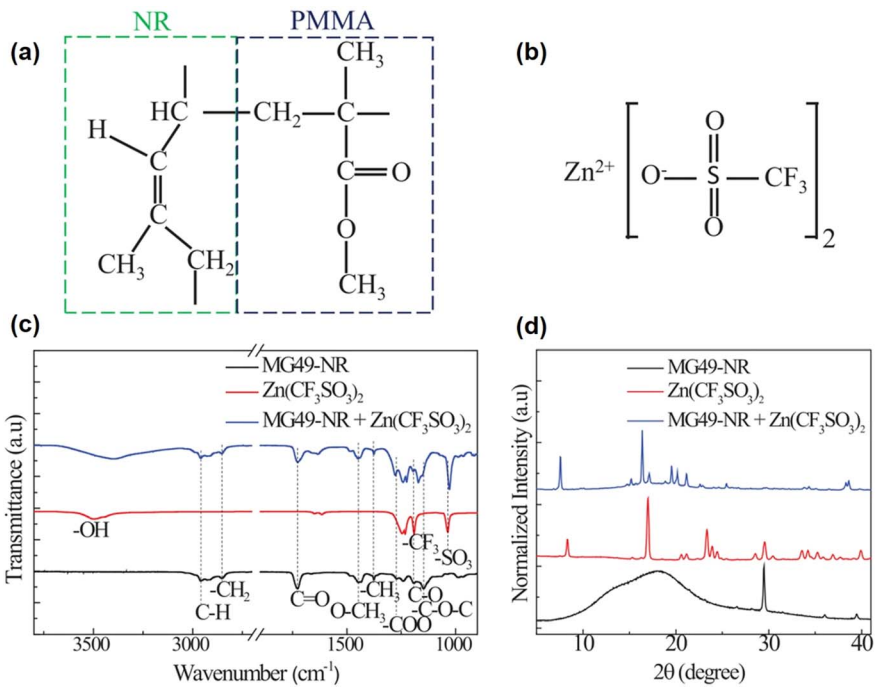

Fig. 9 Schematic of (a) MG_{49}-NR and (b) $Zn(CF_3SO_3)_2$ and (c) attenuated total reflectance FTIR and (d) XRD spectra of the proposed samples. Reproduced with permission from ref. 63 Copyright (2023), Wiley Verlag VCH.

© 2025 The Author(s). Published by the Royal Society of Chemistry

Open Access Article. Published on 05 2025. Downloaded on 2026/5/17 12:30:56.
This article is licensed under a Creative Commons Attribution-NonCommercial 3.0 Unported Licence.

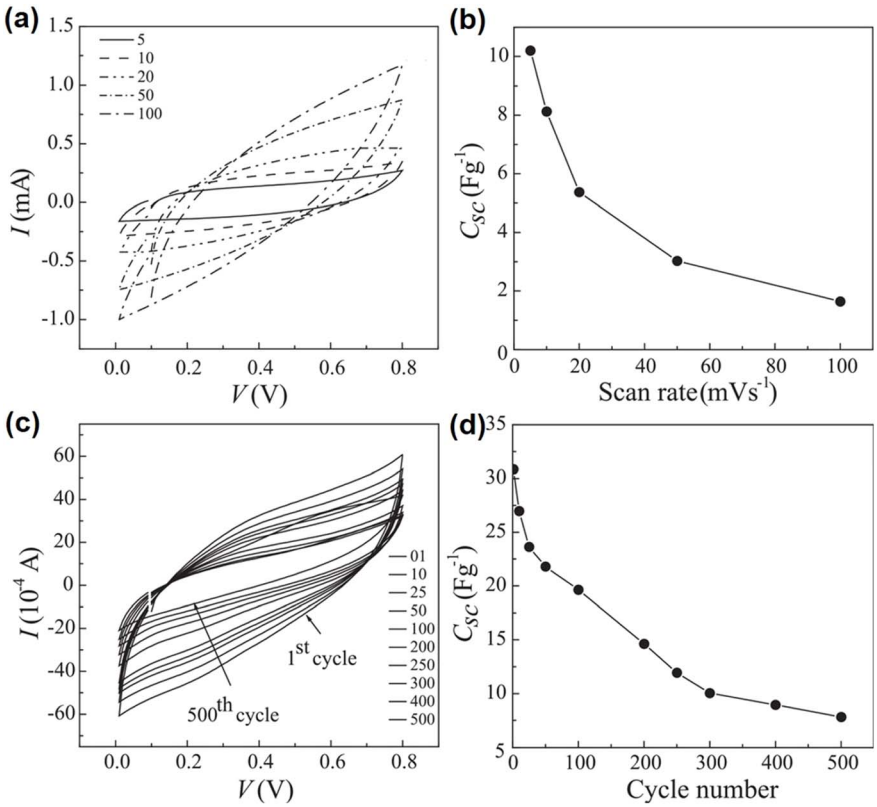

Fig. 10 (a) CV curves at different scan rates; (b) capacitance variation with respect to scan rates; (c) CV curves at different cycle numbers (1 to 500); and (d) plot of variation in the specific capacitance of the single electrode for 500 continuous cycles at a fixed scan rate of 10 mV s^{-1}. Reproduced with permission from ref. 63 Copyright (2023), Wiley-Verlag VCH Ltd.

may be the reason for this nature since at higher scan rates, there will be insufficient time available for the electrolyte ion interaction with the electrode surface. Fig. 10b display the variation in the specific capacitance at different scan rates. The specific capacitance of the supercapacitor is found to be decreased significantly upon increasing the scan rate. The cycling stability of the supercapacitor is examined for 500 continuous CV cycles, and the CV curves obtained at each cycle are depicted in Fig. 10c. From these curves, it can be observed that the area under the curve decreases upon increasing the cycle number and the area becomes very much lower for the 500th cycle when compared to that of the first cycle. The specific capacitance variation at different cycle numbers during the cycling test is plotted in Fig. 10d. A specific capacitance of 30.85 F g^{-1} is obtained at its first cycle, whereas it is only 7.82 F g^{-1} after completing 500 cycles. This deterioration rate is faster in the beginning (say up to 50 cycles) and then it became slow. However, considering the factors such as safety and reduced cost, the polymer electrolyte used in this study is better than the commercially available solid-state electrolytes that utilize organic solvents. The authors of this work evaluated the variation in capacitance from GCD measurements. The GCD measurement was carried out for the supercapacitor for continuous 5000 cycles. A specific capacitance of 12 F g^{-1} is obtained for the first cycle, and it is found to be decreased significantly upon cycling and a specific capacitance of 0.2 F g^{-1} is achieved after completing 5000 cycles. This initial fast reduction in specific capacitance is due to the absence of a perfectly formed interface after fabrication. After some charge–discharge cycles, the device attains maturity and the interface is active. The decrease in specific capacitance in continuous cycles suggests the introduction of ion-pairs and aggregates in electrolyte, depletion of the electrolyte–electrode interface and weakening of the electrolyte. During charge–discharging, ions form pairs, which lead to ion aggregation that does not favour ion migration. Therefore, there is a reduction in the number of ions accumulated at the electrode/electrolyte boundary with overall reduction in specific capacitance. In the first cycle, the energy density attains a value of 1.69 Wh kg^{-1} and it is reduced to 0.02 Wh kg^{-1} after completing 5000 cycles.

Hydrogel electrolytes become a prominent choice as electrolytes for supercapacitor applications due to their salient features such as good flexibility, reduced cost, safety, and biodegradability. Currently, the advancements in energy storage technology demand developing stretchable and flexible devices, but the electrolyte compatibility is a major bottleneck. Hydrogel electrolytes are better alternatives that can resolve these issues. However, balancing the various factors such as ionic conductivity, stretchability, and self-healing capability is still a challenge. Among the various types of matrices developed for solid polymer electrolytes, the epoxidized NR (ENR) has unique features such as soft elastomeric features at room temperature,

Open Access Article. Published on 05 2025. Downloaded on 2026/5/17 12:30:56.
This article is licensed under a Creative Commons Attribution-NonCommercial 3.0 Unported Licence.

adhesiveness, and reduced glass transition temperature (T_g). A T_g of −21 °C for 50 mol% ENR and −43 °C for 25 mol% ENR were obtained.[47] By introducing the ENR in the hydrogel, it introduces the hydrogel with a hydrophobic group, which originates from hydrophobic interactions between cross-linked hydrogels. By the introduction of the hydrophobic segment to the hydrophilic polymer segment for co-polymerization, the hydrophobic segment behaves as a dynamic cross-linking point to the hydrogel.[47] There is a report based on the significance of ENR-related copolymer hydrogel electrolytes for the fabrication of an EDLC.[47] In this study, ENR is copolymerized by acrylamide and acrylic acid. The copolymer hydrogel is prepared by free radical phenomena, and glutaraldehyde is used as a cross-linker. In this work, the hydrogel with chemical cross-linking is prepared through the dispersion of desired quantities of ENR in water. The ENR/water dispersion is mixed with the accurate concentration of acrylamide, acrylic acid, ammonium peroxodisulfate, and glutaraldehyde. Here, glutaraldehyde is used as a cross-linking agent, which makes cross-linking with ENR, acrylamide, and acrylic acid. The prepared mixture is kept under stirring at a temperature of 100 °C and the hydrogel network is introduced by radical polymerization after a time period of 20 minutes. This hydrogel is further immersed in 1 M Na_2SO_4 at a temperature of 25 °C for different time intervals such as 0, 24, 48, and 72 h, and these samples are labelled as S0, S24, S48, and S72, respectively. The hydrogel contains a functional group like amine. By soaking in a Na_2SO_4 solution, sulfate ions $(SO_4)^{2-}$ having a negative charge are interacted with positively charged groups in the polymer chain in a hydrogel, like an amine group. This interaction produces ionic bonds that cross-linking polymer chains lead to a highly rigid structure in the hydrogel. The proposed process indicates the formation of a second network, named it chain entanglement interaction and the resultant structure is not compulsorily a separate network within the hydrogel, but produces modification in the existing network structure by introducing new cross-linking. The morphological features of freeze-dried S0, S24, S48, and S72 samples are examined. The S0 sample exhibits a porous architecture, and it is formed through chemical cross-linking in ENR, acrylamide and acrylic acid with glutaraldehyde. By introducing salt to the prepared hydrogel, S24, S48, and S72 have a compact architecture with few pores. There exists a significant reduction in pore size due to the interaction between the salt and the polymer during the immersion process. The ions produced from salt replace water present in the hydrogel since they are highly attracted by a polymer chain, thus the surface of hydrogel becomes shrunk and collapses. In the energy-dispersive X-ray spectroscopic analysis, it was found that S0, S24, S48, and S72 contain carbon, nitrogen and oxygen, whereas S24, S48, and S72 samples contain additional amounts of sodium and sulfur. This clearly shows that salt makes a distribution completely in the immersed hydrogel. Further, the electrodes for EDLC are prepared by using a porous material like porous carbon having an adequate surface area. The authors of this work introduced the electrode-active material, CNT, with porous carbons. The features of CNTs such as large surface area, good electronic conductivity, ballistic electron transport, and mesoporous structure make them attractive electrode-active materials for supercapacitor application. By incorporating CNTs with porous carbons, an improvement in the electrochemical charge storage is expected due to the synergistic effect of both the electrode-active materials. EDLC is fabricated with two identical electrodes sandwiched by the hydrogel electrolyte in between two stainless-steel current collectors. Four EDLCs are fabricated with each type of hydrogen electrolytes developed in this study such as S0, S24, S48, and S72 and the as-fabricated EDLCs are labelled as PC/S0/PC, PC/S24/PC, PC/S48/PC, and PC/S72/PC. CV analysis is performed for these four EDLCs within a potential window of 0.0 to 1.0 V at different scan rates, ranging from 5 to 100 mV s^{-1}, as depicted in Fig. 11a–d. The CV curves depict the typical box-type nature, representing EDL charge storage. The rectangular shape is found to be unaltered at different scan rates, which shows the good rate capability of the EDLC. The PC/S0/PC exhibits a low area under the CV curve, at each scan rate, when compared to that of the other three EDLCs. By increasing the scan rate from 5 to 100 mV s^{-1}, the specific capacitance of EDLCs is reduced from 21.54 to 5.58 F g^{-1} (by 75%), 45.73 to 16.74 F g^{-1} (by 64%), 48.29 to 18.30 F g^{-1} (by 62%), and 47.11 to 18.64 F g^{-1} (by 61%) for PC/S0/PC, PC/S24/PC, PC/S48/PC, and PC/S72/PC, respectively.

GCD measurements are carried out for the four EDLCs within a potential window of 0.0–1.0 V at different current densities such as 100, 200, 300, 400, and 500 mA g^{-1}, and the GCD profiles are shown in Fig. 12. At higher current densities, the EDLCs exhibit short discharge intervals as the time required for the electrochemical reaction is not sufficient enough to take part in the charge storage. At lower current densities, electrolyte ions receive enough time to penetrate through the porous structure of the electrode, thus an enhanced interaction between the electrode/electrolyte is achieved. Among the four EDLCs fabricated, the PC/S48/PC exhibits a higher discharging time in comparison with the other three EDLCs. The specific capacitance for the EDLCs from the GCD curves was calculated to be 30.15, 47.50, 55.65, and 52.01 F g^{-1} for the PC/S0/PC, PC/S24/PC, PC/S48/PC, and PC/S72/PC, respectively. From the GCD analysis, it can be observed that PC/S48/PC exhibits superior charge storage, which may be due to the optimized immersion time of hydrogel in the salt solution. By increasing the immersion time to 48 h, the improvement in supercapacitor performance arises from higher ionic conductivity imparted by the hydrogel electrolyte, thereby allowing more time for Na^+ and SO_4^{2-} ion permeation into the hydrogel.

From the Ragone plot analysis of EDLCs, the authors of this work observed that PC/S48/PC delivers a higher energy density in the range of 3.78 to 7.50 Wh kg^{-1} and power density in the range of 98.56 to 461.22 W kg^{-1}. From the cyclic stability analysis, it is found that PC/S48/PC exhibits a high capacitive retention of ~90% even after 3500 cycles, indicating an efficient reversibility of the EDLC. The self-healing character of S48 hydrogel was further evaluated, and it is demonstrated in Fig. 13a. The hydrogel is initially cut from the middle portion, and the separated surface of the ruptured hydrogel sample is left in a closed case at a temperature of 60 °C. To avoid potential

© 2025 The Author(s). Published by the Royal Society of Chemistry

Open Access Article. Published on 05 2025. Downloaded on 2026/5/17 12:30:56.
This article is licensed under a Creative Commons Attribution-NonCommercial 3.0 Unported Licence.

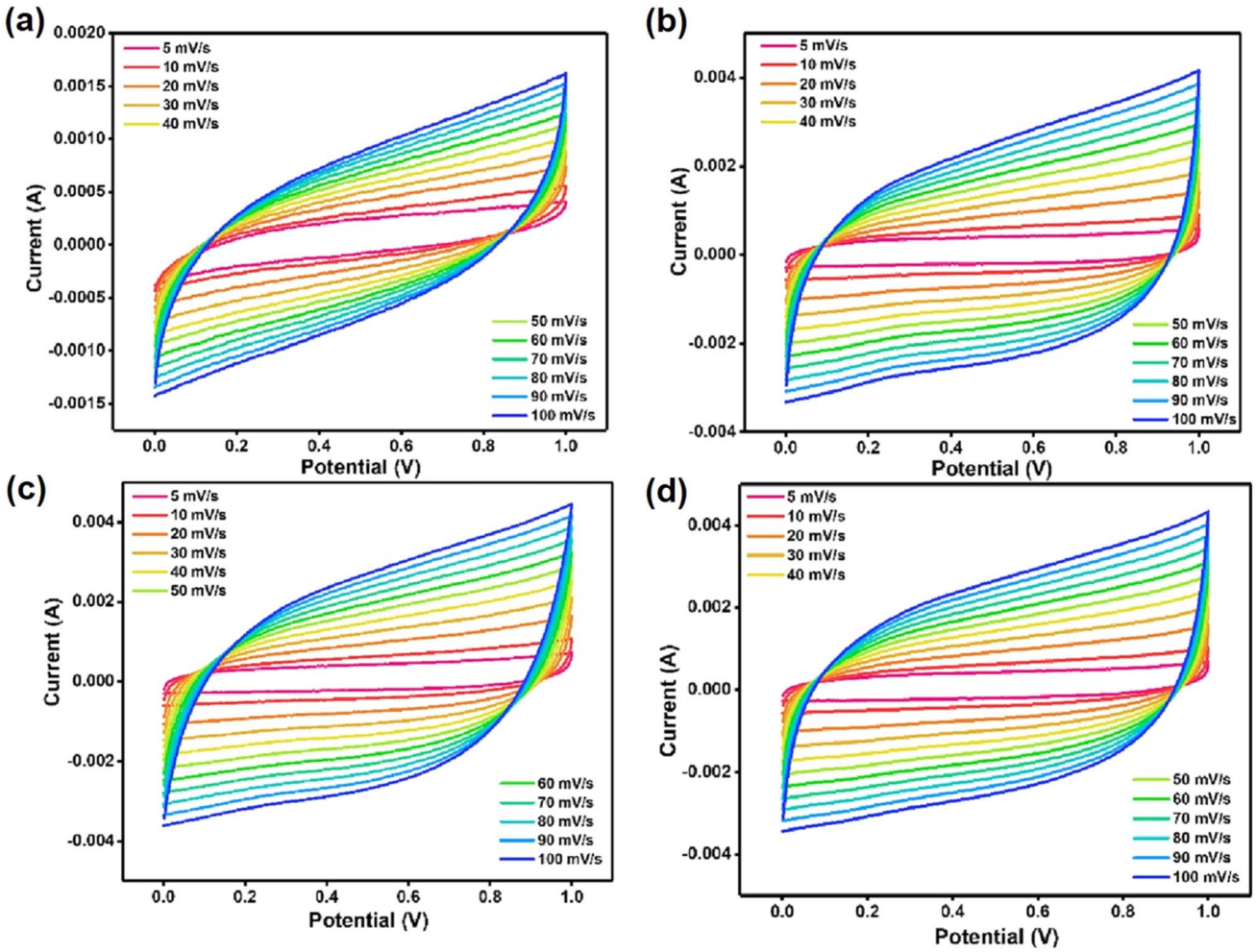

Fig. 11 CV curves at different scan rates of symmetric EDLCs: (a) PC/S0/PC, (b) PC/S24/PC, (c) PC/S48/PC, and (d) PC/S72/PC. Reproduced with permission from ref. 47 Copyright (2023), Elsevier Inc.

separation of faces in thermal treatment, pressure is introduced to facilitate a close contact with two faces of the cut cross-section. After 30 minutes, the hydrogel is capable of recombining and it merged into a single piece. This corresponds to abundant hydrogen bonds present between the polar groups of the polymer side chain in the hydrogel and crosslinking of ions due to Na_2SO_4 in the proposed hydrogel electrolyte. In addition to this, a hydrogel with 0.5 cm thickness and 2.5 cm length is examined for its ability to stretch and elongate. S48 and S72 are kept for elongation tests with hand, and it is given in Fig. 13b, to evaluate their efficiency as a hydrogel electrolyte. The S48 hydrogel has the capability to stretch towards 550% of its initial length (Fig. 13b(i)), whereas the S72 hydrogel elongates to 500% of initial length (Fig. 13b(ii)). This study shows that a higher immersion time makes hydrogels break and an optimized processing time exists during the preparation to attain the best results. From these results, it can be inferred that the supercapacitors fabricated with hydrogel electrolytes are potential candidates for application in electronic wearables. Stretchable and wearable electronic devices require energy storage devices such as supercapacitors to power them.

An intrinsically stretchable supercapacitor electrode consists of an acrylate rubber (ACM)/MWCNT film composite supported by conductive polymers such as poly(1,5-diaminoanthraquinone) (PDAA) and PANI.[64] In the proposed stretchable electrodes, ACM functions as a stretchable matrix, which prominently improves electrode stretchability and affinity towards the organic electrolyte. The MWCNT provides sufficient conductive pathways and promotes the electrodeposition of the conducing polymer PANI. To increase the electrochemical performance as a stretchable electrode, conducting polymers such as PDAA and PANI are electrodeposited over the ACM/MWCNT film to fabricate stretchable electrodes for supercapacitors. The electropolymerization procedure is performed in a polar organic solvent, which benefits in penetrating the monomer into the ACM matrix, which ensures a uniform coating of conducting polymer over the MWCNT surface. The FESEM image of the ACM/MWCNT@PDAA film shows that the MWCNT maintains their intertwined network structure, with the increase in diameter from 20 to 40 nm. It is found that the MWCNT possesses a rough morphology by the incorporation of PDAA nanoparticles, which confirms the decoration of PDAA onto the MWCNT

Open Access Article. Published on 05 2025. Downloaded on 2026/5/17 12:30:56.
This article is licensed under a Creative Commons Attribution-NonCommercial 3.0 Unported Licence.

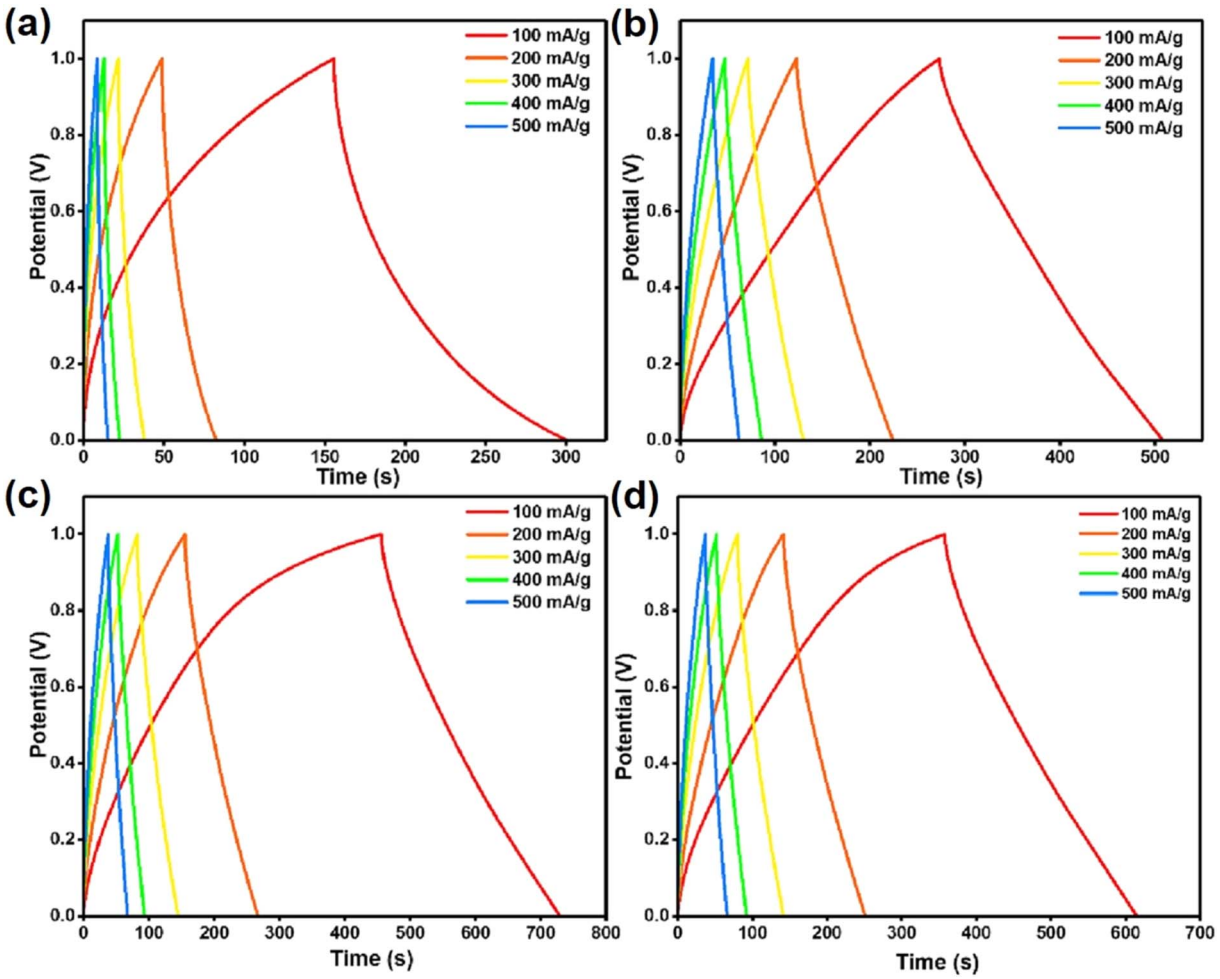

Fig. 12 GCD curves at different scan rates of symmetric EDLCs: (a) PC/S0/PC, (b) PC/S24/PC, (c) PC/S48/PC, and (d) PC/S72/PC. Reproduced with permission from ref. 47 Copyright (2023), Elsevier Inc.

surface. To evaluate the optimal charge density polymerization in ACM/MWCNT@PDAA, the specific capacitance of ACM/MWCNT@PDAA obtained at different charge densities is evaluated using CV and GCD analysis. By increasing the charge density of polymerization from 1 to 4 C cm^{-2}, the CV curve exhibited by ACM/MWCNT@PDAA exhibits a large integral area with prominent redox peaks. The GCD curves possess long discharge time intervals within a negative potential window of −1.8 to −0.45 V, representing higher specific capacitance with more deposition of PDAA. From the GCD measurement, the specific capacitance of ACM/MWCNT@PDAA obtained at a charge density of 2 C cm^{-2} is found to be 20.2 F cm^{-3} at a current density of 1 mA cm^{-2}, which is eight times greater than that of the ACM/MWCNT film (2.5 F cm^{-3}). Moreover, the supercapacitor electrode has efficient rate performance characteristics with a capacitance retention of 58% at a current density of 20 mA cm^{-2}. In addition to this, the specific capacitance of ACM/MWCNT@PDAA obtained at a charge density of 4 C cm^{-2} is high, and it holds an unsymmetrical GCD curve. This is due to the excess amount of deposition introduced by PDAA having a dense structure, which blocks the movement of electrolyte ions. From this evaluation of rate capability and specific capacitance, the ACM/MWCNT@PDAA electrode obtained at a charge density of 2 C cm^{-2} is considered as optimal to assemble an asymmetric supercapacitor. The mechanical properties of the ACM/MWCNT@PDAA electrode are also evaluated, and it possesses a tensile strength of 12.8 MPa and an elongation of 92% at break, which represents an efficient stretchability. In order to increase the specific capacitance of the supercapacitor electrode, PANI is electrodeposited onto the ACM/MWCNT at different polymerization charge densities such as 1, 3, and 5 C cm^{-2} and the as-obtained electrode is labelled as the ACM/MWCNT@PANI stretchable cathode. The FESEM analysis of the ACM/MWCNT@PANI electrode shows that PANI makes an efficient growth over the MWCNT surface, which increases the diameter to 30–50 nm. To match the anode prepared using ACM/MWCNT@PDAA, the charge balance relationship $q^{+} = q^{-}$ is considered. The electrochemical features of the ACM/MWCNT@PANI cathode are investigated in a three-electrode cell arrangement with a 1 M Et_4NBF_4 electrolyte. By increasing the charge density from 1 to 5 C cm^{-2}, the CV curve exhibits a large integral area within a potential window of −0.45–0.9 V. The specific capacitance of the ACM/MWCNT@PANI electrode prepared at a polymerization charge density of 3 C cm^{-2} achieves

© 2025 The Author(s). Published by the Royal Society of Chemistry

Open Access Article. Published on 05 2025. Downloaded on 2026/5/17 12:30:56.
This article is licensed under a Creative Commons Attribution-NonCommercial 3.0 Unported Licence.

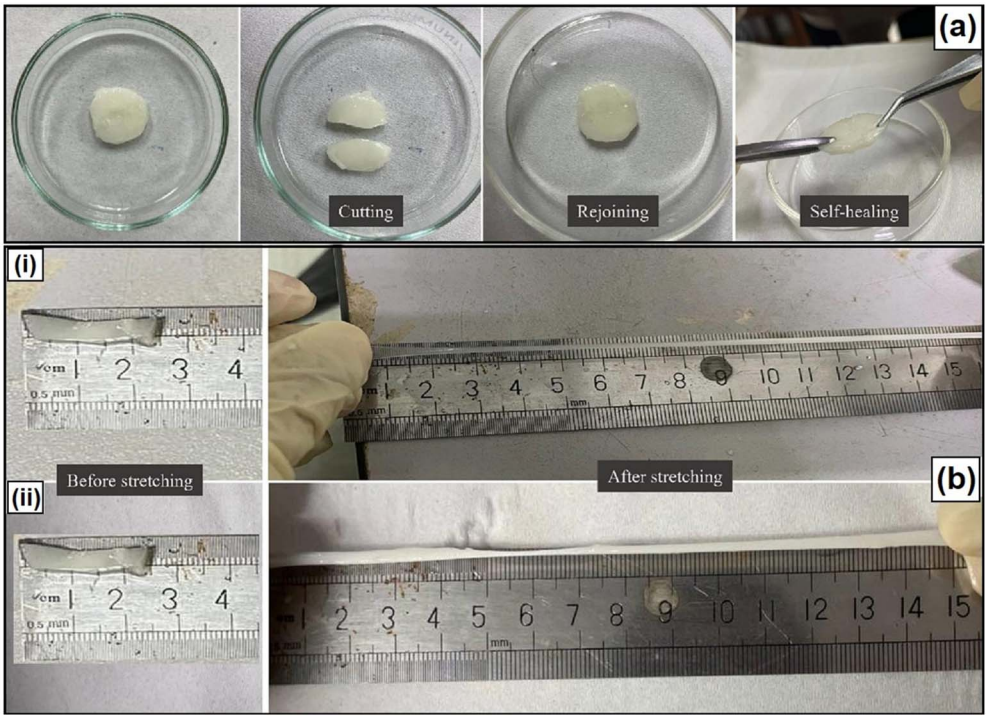

Fig. 13 (a) Digital images of the S48 hydrogel sample. After cutting into two pieces and pressing together for a duration of 30 minutes at 60 °C, it merges into a single piece and (b) photograph of hydrogels before and after stretching exercise for (i) S48 and (ii) S72. Reproduced with permission from ref. 47 Copyright (2023), Elsevier Inc.

17.2 F cm^{-3} at a current density of 1 mA cm^{-2}. Further, the electrochemical evaluation of the asymmetric supercapacitor assembled using ACM/MWCNT@PANI//ACM/Et_4NBF_4–AN//ACM/MWCNT@PDAA is carried out. The CV curves display a symmetrical shape during the reduction/oxidation, representing an efficient pseudocapacitive character of the asymmetric supercapacitor. The GCD curve possesses highly symmetrical triangular shaped charge/discharge curves with a very small voltage drop. The volumetric specific capacitance of asymmetric supercapacitor is calculated to be 1.9 F cm^{-3} at a current density of 30 mA cm^{-2}. The asymmetric supercapacitor exhibits a reduced ohmic resistance and charge-transfer resistance of 3.1 and 2.1 Ω, respectively. This is due to the efficient affinity and contact generated between the stretchable electrodes and organic polymer electrolytes coupled with the rapid charge transport and diffusion of ions. The asymmetric supercapacitor exhibits an efficient energy density of 2.14 mWh cm^{-3}. A high capacitance retention of 86% is obtained when cycled at a current density of 30 mA cm^{-2}, with efficient cyclic stability during static and 50% strain condition after 300 stretching cycles. These results indicate the efficiency of fabricated supercapacitors in stretchable electronics. The polymeric gel electrolyte possesses efficient characteristics such as high ionic conductivity and wide electrochemical potential window. By utilizing the features of NRL, a gel electrolyte is proposed to assemble a symmetric supercapacitor. Using a solution casting approach, a gel polymer electrolyte with 30% PMMA-grafted NR, which is doped with ammonium triflate and plasticized by ethylene carbonate is reported.[65] After completion of the plasticized procedure, the gel polymer electrolyte possesses a room temperature conductivity of 9.61 × 10^{-4} S cm^{-1} at a composition of 26 : 14 : 60 (in wt%) for grafted NR : ammonium triflate : ethylene carbonate. From linear sweep voltammogram analysis, it is observed that the gel polymer electrolyte has an electrochemically stable operating voltage of 2.7 V. The symmetric supercapacitor device fabricated using this gel polymer electrolyte exhibits a specific capacitance of 32 F g^{-1} with a coulombic efficiency of 90%. A flexible carbon black-filled conductive composite as an excellent electrode for the substitution of graphite in the electrochemical preparation of PANI-based nanocomposite is reported for supercapacitor applications.[66] Elastomeric nanocomposites of acrylonitrile butadiene copolymer (NBR) as the matrix having various classes of carbon black fillers such as N660, N330, and XC72 (VULCAN®XC-72) are synthesized by a melt mixing approach. Among these different composites prepared, the NBR-XC72 nanocomposite exhibits good electronic conductivity and mechanical properties. In general, a higher conductivity is required for electrode-active materials and electronically conducting polymers are the best option to enhance the conductivity when the composites are prepared. The electrochemical polymerization of PANI was performed using two different classes of PANI samples. The specific capacitance delivered by PANI with graphite is 380 F g^{-1} in comparison to the composite electrode (213 F g^{-1}) at a current density of 1 A g^{-1}. After 1000 charge/discharge cycles, the capacitance retention for PANI with NBR-XC72 was 90%, which is higher than the PANI/graphite nanocomposite (the capacitance retention was 81%). The flexible nature in the elastomeric composite electrode makes it a prominent one for PANI

Open Access Article. Published on 05 2025. Downloaded on 2026/5/17 12:30:56.
This article is licensed under a Creative Commons Attribution-NonCommercial 3.0 Unported Licence.

Table 1 Summary of the electrochemical performances of rubber nanocomposite-based supercapacitor electrodes reported in the literature

Electrode	Synthesis method	Morphology	Specific capacitance (F g^{-1})	Ref.
GO/NRL	Electrochemical exfoliation	Rose petal-like	103.70	57
GO/NRL	One-step approach	Sheet-like	107.00	58
rGO/NRL	Stirring and ultrasonication	Sheet-like	95.00	60
GO/NRL	Electrochemical exfoliation	Wavy	30.00	62
Methyl-grafted NRL	Solvent casting	Layered	30.85	63
ENR copolymerized with acrylamide and acrylic acid	Cross-linking	Porous	47.11	47

electrochemical synthesis, as well as to other nanomaterials. The electrochemical performances of supercapacitor electrodes prepared using rubber nanocomposites are summarized in Table 1. From this table, it is clear that the rubber nanocomposite-based electrodes are potential candidates for application in supercapacitors with high specific capacitance.

5. Challenges and future perspectives

From the present study, it is clear that rubber nanocomposites are potential candidates for supercapacitors. Rubber nanocomposites function as additives in electrode-active materials or electrolytes. The elastic strength of rubber nanocomposites is the most prominent property, which has gained the research interest for application in flexible supercapacitors. Elasticity, flexibility, tensile strength, and adhesion to environmental conditions during processing are the salient features of NR and its derivatives for supercapacitor electrode fabrication. The supercapacitors fabricated using rubber nanocomposites find potential application in wearable electronic devices to supply them power. From the present review, we can find that there are only a limited number of publications based on rubber nanocomposite electrodes for supercapacitor applications. More research works have to be conducted in the field of rubber nanocomposites to understand their peculiar features that can be made use for flexible supercapacitors. For the preparation of rubber nanocomposite-based supercapacitor electrodes, electrode-active materials such as electronically conducting polymers,[67,68] layered transition metal sulfides,[69–71] carbon nitrides,[72] MXenes,[73–75] transition metal oxides,[76,77] and metal phosphates[78,79] are promising candidates due to their excellent charge storage capability and stability towards harsh chemical and electrochemical environments. Different types of polymer additives can be used during the preparation of rubber nanocomposites in order to enhance the electronic conductivity, elasticity, mechanical strength, *etc.* The future outlook of rubber nanocomposites for supercapacitor applications is depicted in Fig. 14. Easy and rapid synthesis routes are extremely important for the scalability of synthesizing rubber nanocomposites. As mentioned previously, the preparation of rubber nanocomposites with other electrode-active materials opens-up new avenues for developing high-performance supercapacitors for wearable electronic applications. Most importantly, the rubber nanocomposite-based supercapacitor electrode should possess high specific capacitance, good stretchability, and long-term cycle life. Novel strategies such as heteroatom doping and defect engineering provide a facile route to enhance the electrochemical charge storage properties of the rubber nanocomposite-based supercapacitor electrodes. A thorough understanding on the various properties of rubber nanocomposites is mandatory to develop electrodes for high-performance supercapacitors for futuristic applications such as wearable electronics.

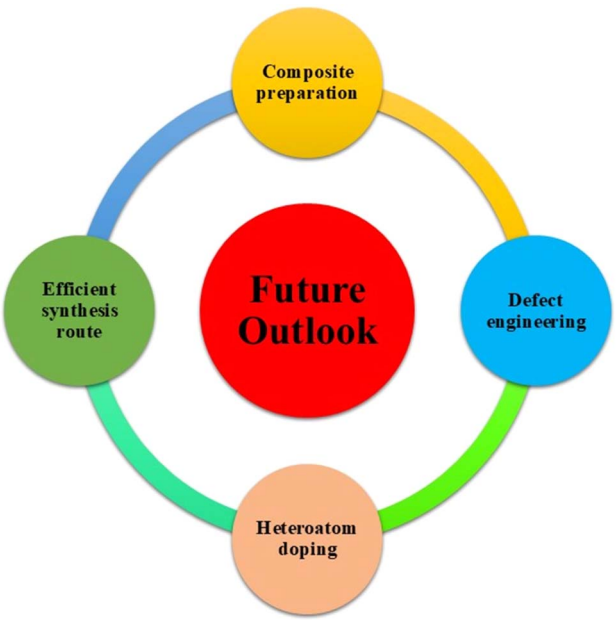

Fig. 14 Future outlook of rubber-based nanocomposites in supercapacitors.

6. Summary and outlook

In this review article, we discussed the recent developments of rubber nanocomposite-based electrodes for supercapacitor applications. The features of rubber nanocomposites such as electronic, mechanical, and optical properties were reviewed at first followed by various methods adopted for their synthesis. Methods such as solution mixing, mechanical/melt mixing, and latex mixing are explained with the help of relevant characterization tools such as SEM imaging, HRTEM imaging, Raman spectroscopy, and FTIR spectroscopy. The main focus was given to the electrochemical performances of rubber nanocomposite-based electrodes for application in supercapacitors,

© 2025 The Author(s). Published by the Royal Society of Chemistry

Open Access Article. Published on 05 2025. Downloaded on 2026/5/17 12:30:56.
This article is licensed under a Creative Commons Attribution-NonCommercial 3.0 Unported Licence.

electrochemical performance evaluation was conducted using CV analysis, GCD measurements, *etc.*, and the performance parameters such as specific capacitance, energy density, and power density were calculated. The effects of the addition of filler materials such as GO, rGO, SWCNTs, and MWCNTs on the performance of rubber nanocomposites were evaluated using established electrochemical performance evaluation tools. Like other nanocomposites, the optimal concentration of filler materials in rubber nanocomposites was found to be critical in determining the electrochemical performance parameters of the supercapacitor electrode. The flexibility and long-term cycling stability of the rubber nanocomposite electrodes were evaluated, which show good durability and versatility for commercial applications. Stretchable supercapacitors prepared using rubber nanocomposite electrodes were found to be the best candidates for supercapacitor applications as they possess high specific capacitance and long cycle life.

Data availability

The data discussed herein can be found in the referenced articles.

Author contributions

Susmi Anna Thomas: data curation, software, writing – original draft, writing – weview & editing, software, visualization. Jayesh Cherusseri: conceptualization, writing – original draft, writing – review & editing, visualization. Deepthi N. Rajendran: supervision, visualization.

Conflicts of interest

The authors declare that they have no known competing financial interests or personal relationships that could have appeared to influence the work reported in this paper.

References

1 D. Kumar, *et al.*, Nanocarbon assisted green hydrogen production: Development and recent trends, *Int. J. Hydrogen Energy*, 2023, **50**, 118–141.
2 S. A. Thomas, J. Cherusseri and D. N. Rajendran, Loofah Sponge: A Sustainable Material for Wastewater Desalination, *RSC Sustainability*, 2025, DOI: **10.1039/D5SU00043B**.
3 S. A. Thomas, J. Cherusseri and D. N. Rajendran, Recent advancements on carbon fibers-based sustainable electrodes for flexible and wearable supercapacitors, *RSC Sustainability*, 2024, **2**, 2403–2443.
4 S. A. Thomas and J. Cherusseri, Boron Carbon Nitride (BCN): Emerging Two-Dimensional Nanomaterial for Supercapacitors, *J. Mater. Chem. A*, 2023, **11**, 23148–23187.
5 N. Rosen, *et al.*, Assessment of the Potential of Electrochemical Steps in Direct Air Capture through Techno-Economic Analysis, *Energy Fuels*, 2024, **38**(16), 15469–15481.
6 S. A. Thomas, J. Cherusseri and D. N. Rajendran, Rapid synthesis of hierarchical cobalt disulfide nanostructures by microwave-assisted hydrothermal method for high performance supercapatteries, *ACS Appl. Electron. Mater.*, 2024, **6**(6), 4321–4335.
7 M. R. Pallavolu, *et al.*, Scalable synthesis of binder-free hierarchical MnCo2O4 nanospikes/Ni (OH) 2 nanosheets composite electrodes for high-capacity supercapatteries, *J. Energy Storage*, 2023, **73**, 108999.
8 R. R. Judkins, W. Fulkerson and M. K. Sanghvi, The dilemma of fossil fuel use and global climate change, *Energy Fuels*, 1993, **7**(1), 14–22.
9 C. Esarte and J. Delgado, Influence of heating oil formulation on the combustion and emissions of domestic condensing boilers using fossil fuel and renewable fuel mixtures, *Energy Fuels*, 2018, **32**(10), 10106–10113.
10 R. García-Contreras, *et al.*, Fuel Lubricity Assessment of Fossil and Synthetic Paraffinic Kerosene to Be Used in Reciprocating Engines, *Energy Fuels*, 2024, **38**(19), 18652–18659.
11 L. M. Gandía, *et al.*, Renewable hydrogen production: performance of an alkaline water electrolyzer working under emulated wind conditions, *Energy Fuels*, 2007, **21**(3), 1699–1706.
12 M. Sudiro and A. Bertucco, Synthetic fuels by a limited CO2 emission process which uses both fossil and solar energy, *Energy Fuels*, 2007, **21**(6), 3668–3675.
13 S. A. Thomas, *et al.*, Graphitic carbon nitride (g-C3N4): Futuristic material for rechargeable batteries, *J. Energy Storage*, 2023, **68**, 107673.
14 A. T. Irewale, *et al.*, Morphological and Chemical Profiling of Biochar Derived from Invasive Aquatic Weed Towards Bio-nanofertilizer Development, *RSC Sustainability*, 2025, DOI: **10.1039/D5SU00052A**.
15 S. A. Thomas, *et al.*, Water-in-salt" electrolyte—toward high-voltage aqueous supercapacitors, in *Supercapacitors*, Elsevier, 2024, pp. 289–315.
16 J. Cherusseri, Polymer-Ionic Liquid Gel Electrolytes for Lithium-Ion Batteries, in *Polymer Electrolytes for Energy Storage Devices*, CRC Press, 2021, pp. 235–253.
17 S. A. Thomas, J. Cherusseri and D. N. Rajendran, A Minireview on Polyurethane-Based Flexible Electrodes for Wearable Supercapacitors: Strategies, Syntheses and Electrochemical Performance Evaluations, *Energy Fuels*, 2024, **39**(1), 2–18.
18 S. A. Thomas, *et al.*, Strategically-Designed Environment-Friendly Tin-Based Electrodes for Sustainable Supercapatteries with High Specific Capacity, *Electrochim. Acta*, 2025, 145846.
19 S. A. Thomas, Layered two-dimensional black phosphorous-based hybrid electrodes for rechargeable batteries, *J. Energy Storage*, 2023, **73**, 109068.
20 S. A. Thomas, *et al.*, Polyoxometalates and redox-active molecular clusters for supercapacitors, in *Supercapacitors*, Elsevier, 2024, pp. 221–243.
21 J. Nallapureddy, *et al.*, Hierarchical nickel molybdenum sulfide whisker nanoneedles: Binder-free in situ grown

Open Access Article. Published on 05 2025. Downloaded on 2026/5/17 12:30:56.
This article is licensed under a Creative Commons Attribution-NonCommercial 3.0 Unported Licence.

electrodes designed for enhanced supercapattery performance, *J. Energy Storage*, 2025, **123**, 116864.
22 R. K. Mishra, *et al.*, Heterogeneous Integration of 2D Materials with Silicon Complementary Metal Oxide Semiconductor (Si-CMOS) Devices, in *Beyond Si-Based CMOS Devices: Materials to Architecture*, Springer, 2024, pp. 149–179.
23 P. S. Menon, *et al.*, The role of defects in the nonlinear optical absorption behavior of pristine and Co-doped V2O5 layered 2D nanostructures, *J. Alloys Compd.*, 2022, **907**, 164413.
24 J. Mathai, *et al.*, Cr doped ZnO nanoparticles as photocatalyst for the degradation of methylene blue dye, *J. Indian Chem. Soc.*, 2023, **100**(9), 101067.
25 S. A. Thomas, *et al.*, Minireview on Exploring MAX Phases for Hydrogen Energy Storage: Strategies, Development, and Future Perspectives, *Energy Fuels*, 2025, **39**(3), 1460–1478.
26 S. A. Thomas, J. Cherusseri, and D. N. Rajendran, Functionalized Carbon Nanostructures for Hydrogen Storage, in *Handbook of Functionalized Carbon Nanostructures: from Synthesis Methods to Applications*, Springer, 2024, pp. 1471–1509.
27 S. A. Thomas, *et al.*, Functionalized Carbon Nanostructures for Wastewater Treatments, in *Handbook of Functionalized Carbon Nanostructures: from Synthesis Methods to Applications*, Springer, 2024, pp. 1971–2014.
28 S. A. Thomas, *et al.*, Graphitic Carbon Nitride and Their Derivatives, in *Handbook of Functionalized Carbon Nanostructures: from Synthesis Methods to Applications*, Springer, 2024, pp. 1–38.
29 S. Abinaya, *et al.*, Unveiling dynamic insights of nitrogen-doped carbon quantum dots in α-Fe2O3/PANI nanocomposite for supercapattery application, *J. Mater. Sci.*, 2024, **59**(47), 21846–21867.
30 S. N. Akhtar, *et al.*, Ionic polymer metal composites, *Composite Materials: Processing, Applications, Characterizations*, 2017, pp. 223–249.
31 S. A. Thomas, *et al.*, Designing PEDOT-based hybrid electrodes for supercapacitors by electrospinning strategy, *Discover Electrochem.*, 2024, **1**(1), 6.
32 B. Weerasuk, *et al.*, Enhanced dye removal and supercapacitor performance of polyethyleneimine-impregnated activated carbon derived from local eucalyptus biochar, *RSC Sustainability*, 2025, **3**(2), 904–913.
33 V. Aswany, *et al.*, Shape Memory Polymers and Its Composites for 3D-, 4D-, and 5D-Printed Applications, in *Polymer Nanocomposites for 3D, 4D and 5D Printing: Fundamental to Applications*, Springer, 2025, pp. 213–240.
34 R. Mishra, J. Cherusseri, and K. Joseph, Thermal and crystallization behavior of micro and nano fibrillar in-situ composites, in *Micro and Nano Fibrillar Composites (MFCs and NFCs) from Polymer Blends*, Elsevier, 2017, pp. 213–231.
35 M. Zaed, *et al.*, Synthesis and characterization of hierarchical Ti3C2Tx MXene/graphitic-carbon nitride/activated carbon@ luffa sponge composite for enhanced water desalination, *Open Ceram.*, 2024, **19**, 100645.
36 S. Seenivasan, *et al.*, Supercapatteries: unlocking the potential of battery-supercapacitor fusion, *Energy Environ. Sci.*, 2025, **18**, 1054–1095.
37 T. Govindasamy, *et al.*, Modulating the structural and magnetic properties of Fe3O4 NPs for high-performance supercapattery and EMI shielding applications, *J. Energy Storage*, 2024, **79**, 110243.
38 J. Cherusseri, *et al.*, SARS-CoV-2-on-chip for long COVID management, *Biosensors*, 2022, **12**(10), 890.
39 J. Cherusseri, R. Sharma, and K. K. Kar, Nanotechnology advancements on carbon nanotube/polypyrrole composite electrodes for supercapacitors, in *Handbook of Polymer Nanocomposites. Processing, Performance and Application: Volume B: Carbon Nanotube Based Polymer Composites*, Springer, 2015, pp. 479–510.
40 S. A. Thomas and J. Cherusseri, A review of Nb2CT x MXene as an emerging 2D material: synthesis, applications in rechargeable batteries and supercapacitors, progress, and outlook, *Energy Fuels*, 2023, **37**(11), 7555–7576.
41 F. Danafar and M. Kalantari, A review of natural rubber nanocomposites based on carbon nanotubes, *J. Rubber Res.*, 2018, **21**, 293–310.
42 A. Krainoi and K. Boonkerd, Role of natural rubber structure in the electrical conductivity and strain sensor performance of natural rubber/carbon nanotube nanocomposites stabilized by sodium alginate, *Mater. Today Sustainability*, 2024, **26**, 100698.
43 P. Bernal-Ortega, *et al.*, New insight into structure-property relationships of natural rubber and styrene-butadiene rubber nanocomposites filled with MWCNT, *Polymer*, 2020, **201**, 122604.
44 A. Sethulekshmi, A. Saritha and K. Joseph, A comprehensive review on the recent advancements in natural rubber nanocomposites, *Int. J. Biol. Macromol.*, 2022, **194**, 819–842.
45 A. Fakhru'l-Razi, *et al.*, Effect of multi-wall carbon nanotubes on the mechanical properties of natural rubber, *Compos. Struct.*, 2006, **75**(1–4), 496–500.
46 J. Wang, *et al.*, High silica content graphene/natural rubber composites prepared by a wet compounding and latex mixing process, *Polymers*, 2020, **12**(11), 2549.
47 F. Kamarulazam, *et al.*, Stretchable, self-healable and highly conductive natural-rubber hydrogel electrolytes for supercapacitors: Advanced wearable technology, *J. Energy Storage*, 2023, **71**, 108182.
48 X. Wu, *et al.*, Biotemplate synthesis of polyaniline@ cellulose nanowhiskers/natural rubber nanocomposites with 3D hierarchical multiscale structure and improved electrical conductivity, *ACS Appl. Mater. Interfaces*, 2014, **6**(23), 21078–21085.
49 K. Parvathi, B. Bahuleyan and M. Ramesan, Optical, thermal and temperature dependent electrical properties of chlorinated natural rubber/copper alumina nanocomposites for flexible electrochemical devices, *Res. Chem. Intermed.*, 2022, **48**(9), 3897–3914.
50 N. Anhar, *et al.*, Mechanical Properties of Graphene-Rubber Nanocomposites, in *IOP Conference Series: Materials Science and Engineering*, IOP Publishing, 2017.

© 2025 The Author(s). Published by the Royal Society of Chemistry

Open Access Article. Published on 05 2025. Downloaded on 2026/5/17 12:30:56.
This article is licensed under a Creative Commons Attribution-NonCommercial 3.0 Unported Licence.

51 K. Parvathi, B. Bahuleyan and M. Ramesan, Enhanced optical, thermal and electrical properties of chlorinated natural rubber/zinc ferrite nanocomposites for flexible electrochemical devices, *J. Macromol. Sci., Part A: Pure Appl. Chem.*, 2022, **59**(7), 466–479.
52 J. Sharif, *et al.*, Preparation and properties of radiation crosslinked natural rubber/clay nanocomposites, *Polym. Test.*, 2005, **24**(2), 211–217.
53 J. Cherusseri and K. K. Kar, Recent progress in nanocomposites based on carbon nanomaterials and electronically conducting polymers, *Polym. Nanocompos. Inorg. Org. Nanomater.*, 2015, 229–256.
54 W. Kitisavetjit, *et al.*, Influences of carbon nanotubes and graphite hybrid filler on properties of natural rubber nanocomposites, *Polym. Test.*, 2021, **93**, 106981.
55 H. Rajapaksha, K. Perera and K. Vidanapathirana, Suitability of natural rubber-based polymer electrolyte for energy storage, *J. Rubber Res.*, 2021, **24**, 3–12.
56 S. A. Thomas, J. Cherusseri and D. N. Rajendran, Recent progresses in the synthesis and strategic designs of sustainable carbon-based fibrous electrodes for flexible batteries, *RSC Sustainability*, 2025, **3**, 219–242.
57 A. Suriani, *et al.*, A facile one-step method for graphene oxide/natural rubber latex nanocomposite production for supercapacitor applications, *Mater. Lett.*, 2015, **161**, 665–668.
58 M. Nurhafizah, *et al.*, Graphene oxide/low ammonia NRL nanocomposite-based electrode in various electrolyte concentrations: electrical properties and capacitive behavior for supercapacitor, *J. Rubber Res.*, 2020, **23**, 387–393.
59 K. Parvathi, B. Bahuleyan and M. Ramesan, Flexible conductive nanocomposites for electrochemical devices based on chlorinated natural rubber/nickel oxide nanoparticles, *J. Inorg. Organomet. Polym. Mater.*, 2022, **32**(8), 2827–2842.
60 A. Suriani, *et al.*, Electrical enhancement of radiation-vulcanized natural rubber latex added with reduced graphene oxide additives for supercapacitor electrodes, *J. Mater. Sci.*, 2017, **52**, 6611–6622.
61 J. Yoon, J. Lee and J. Hur, Stretchable supercapacitors based on carbon nanotubes-deposited rubber polymer nanofibers electrodes with high tolerance against strain, *Nanomaterials*, 2018, **8**(7), 541.
62 M. Nurhafizah, *et al.*, Low-temperature exfoliated graphene oxide incorporated with different types of natural rubber latex: Electrical and morphological properties and its capacitance performance, *Ceram. Int.*, 2020, **46**(5), 5610–5622.
63 K. S. Perera, *et al.*, Sustainable supercapacitor with a natural rubber-based electrolyte and natural graphite-based electrodes, *Electrochem. Sci. Adv.*, 2023, e2300025.
64 X. Wang, *et al.*, High-performance stretchable supercapacitors based on intrinsically stretchable acrylate rubber/MWCNTs@ conductive polymer composite electrodes, *J. Mater. Chem. A*, 2018, **6**(10), 4432–4442.
65 N. H. M. Zaki, *et al.*, A symmetric supercapacitor based on 30% poly (methyl methacrylate) grafted natural rubber (MG30) polymer and activated carbon electrodes, in *AIP Conference Proceedings*, AIP Publishing, 2017.
66 U. Shankar, S. Bhandari and D. Khastgir, Carbon Black-Filled Nitrile Rubber Composite as a Flexible Electrode for Electrochemical Synthesis of Supercapacitive Polyaniline, *Polym. Compos.*, 2019, **40**(S2), E1537–E1547.
67 S. A. Thomas, J. Cherusseri and D. N. Rajendran, Hierarchical two-dimensional layered nickel disulfide (NiS2)@ PEDOT: PSS nanocomposites as battery-type electrodes for battery-type supercapacitors with high energy density, *Electrochem*, 2024, **5**(3), 298–313.
68 J. Cherusseri, *et al.*, Polymer-based composite materials: characterizations, *Composite Materials: Processing, Applications, Characterizations*, 2017, pp. 37–77.
69 S. A. Thomas and J. Cherusseri, Strategically designing layered two-dimensional SnS2-based hybrid electrodes: A futuristic option for low-cost supercapacitors, *J. Energy Chem.*, 2023, **85**, 394–417.
70 S. A. Thomas, J. Cherusseri and D. N. Rajendran, Nickel Disulfide (NiS2): A Sustainable Low-Cost Electrode Material for High-Performance Supercapacitors, *Energy Technol.*, 2024, **12**(7), 2400138.
71 S. A. Thomas, J. Cherusseri and D. N. Rajendran, Rapid Synthesis of Hierarchical Tin Disulfide (SnS2) Nanostructures by a Microwave-Assisted Hydrothermal Method for High-Performance Supercapatteries, *ACS Appl. Electron. Mater.*, 2024, **6**(5), 3346–3361.
72 S. A. Thomas, *et al.*, Boron carbon nitride (BCN): an emerging two-dimensional material for rechargeable batteries, *Energy Fuels*, 2024, **38**(15), 13704–13721.
73 S. A. Thomas and J. Cherusseri, Recent Advances in Synthesis and Properties of Zirconium-Based MXenes for Application in Rechargeable Batteries, *Energy Storage*, 2023, e475.
74 B. Richard, *et al.*, Minireview on Fluid Manipulation Techniques for the Synthesis and Energy Applications of Two-Dimensional MXenes: Advances, Challenges, and Perspectives, *Energy Fuels*, 2023, **37**(10), 6999–7013.
75 M. Zaed, *et al.*, Unlocking desalination's potential: Harnessing MXene composite for sustainable desalination, *Chem. Eng. J.*, 2024, **500**, 156910.
76 S. A. Thomas, J. Cherusseri and M. Khalid, A comprehensive review on tungsten oxide nanostructures-based electrochromic supercapacitors and machine learning models for design and process parameter optimization, *Energy Storage*, 2023, **5**(8), e499.
77 S. A. Thomas, *et al.*, Translation of supercapacitor technology from laboratory scale to commercialization, in *Supercapacitors*, Elsevier, 2024, pp. 371–395.
78 J. Cherusseri, *et al.*, Rapid synthesis of cobalt manganese phosphate by microwave-assisted hydrothermal method and application as positrode material in supercapatteries, *Sci. Rep.*, 2024, **14**(1), 26550.
79 A. A. Kulkarni, *et al.*, Transition metal phosphates: a paradigm for electrochemical supercapacitors, *J. Electroanal. Chem.*, 2023, **948**, 117795.